Restraint of the G2/M Transition by the SR/RRM Family mRNA Shuttling Binding Protein SNXA^{HRB1} in *Aspergillus nidulans*

Steven W. James,*[,1] Travis Banta,[†] James Barra,* Lorela Ciraku,* Clifford Coile,[†] Zach Cuda,[†] Ryan Day,[†] Cheshil Dixit,[†] Steven Eastlack,[†] Anh Giang,[†] James Goode,[†] Alexis Guice,[†] Yulon Huff,[†] Sara Humbert,[†] Christina Kelliher,* Julie Kobie,* Emily Kohlbrenner,* Faustin Mwambutsa,[†] Amanda Orzechowski,* Kristin Shingler,* Casey Spell,[†] and Sarah Lea Anglin[†,1]

*Biology Department, Gettysburg College, Gettysburg, Pennsylvania 17325, and [†]Biology Department, Millsaps College, Jackson, Mississippi 39210

ABSTRACT Control of the eukaryotic G2/M transition by CDC2/CYCLINB is tightly regulated by protein–protein interactions, protein phosphorylations, and nuclear localization of CDC2/CYCLINB. We previously reported a screen, in *Aspergillus nidulans*, for extragenic suppressors of *nimX2*^{cdc2} that resulted in the identification of the cold-sensitive *snxA1* mutation. We demonstrate here that *snxA1* suppresses defects in regulators of the CDK1 mitotic induction pathway, including *nimX2*^{cdc2}, *nimE6*^{cyclinB}, and *nimT23*^{cdc25}, but does not suppress G2-arresting *nimA1*/*nimA5* mutations, the S-arresting *nimE10*^{cyclinB} mutation, or three other G1/S phase mutations. *snxA* encodes the *A. nidulans* homolog of *Saccharomyces cerevisiae* Hrb1/Gbp2; nonessential shuttling messenger RNA (mRNA)-binding proteins belonging to the serine-arginine-rich (SR) and RNA recognition motif (RRM) protein family; and human heterogeneous ribonucleoprotein-M, a spliceosomal component involved in pre-mRNA processing and alternative splicing. *snxA*^{Hrb1} is nonessential, its deletion phenocopies the *snxA1* mutation, and its overexpression rescues *snxA1* and *ΔsnxA* mutant phenotypes. *snxA1* and a second allele isolated in this study, *snxA2*, are hypomorphic mutations that result from decreased transcript and protein levels, suggesting that *snxA* acts normally to restrain cell cycle progression. SNXA^{HRB1} is predominantly nuclear, but is not retained in the nucleus during the partially closed mitosis of *A. nidulans*. We show that the *snxA1* mutation does not suppress *nimX2* by altering NIMX2^{CDC2}/NIME^{CYCLINB} kinase activity and that *snxA1* or *ΔsnxA* alter localization patterns of NIME^{CYCLINB} at the restrictive temperatures for *snxA1* and *nimX2*. Together, these findings suggest a novel and previously unreported role of an SR/RRM family protein in cell cycle regulation, specifically in control of the CDK1 mitotic induction pathway.

CONTROL of the eukaryotic G2/M transition by protein kinases has been widely studied and is highly conserved among all eukaryotes from the budding and fission yeasts and filamentous fungi to metazoans (for review, see Ma and Poon 2011). The CDK1/CYCLINB protein kinase complex is a major regulator of this transition in all eukaryotes and is responsible for the phosphorylations of numerous proteins, leading to massive nuclear and cytoplasmic reorganizations that regulate mitosis (for review, see Lindqvist *et al.* 2009). The complex itself is tightly regulated, both temporally and spatially, to allow mitotic entry.

Although CDK1/CYCLINB activity is essential for mitotic entry in all eukaryotes, structural differences in the nucleus in various organisms result in "open" mitosis (more complex eukaryotes) or "closed" mitosis (budding yeasts); these differences likely affect the temporo-spatial functioning of CDK1/CYCLINB. The partially closed mitosis of the filamentous fungus *Aspergillus nidulans* is an evolutionary intermediate between open and closed mitoses and provides a system for studying mitotic entry in organisms intermediate between budding yeasts and more complex eukaryotes. The nuclear pore complexes in *A. nidulans* partially disassemble at mitotic entry (they are "partially closed"), and proteins not specifically retained in the nucleus diffuse out of the partially closed

doi: 10.1534/genetics.114.167445
Manuscript received June 18, 2014; accepted for publication July 31, 2014; published Early Online August 7, 2014.
Supporting information is available online at http://www.genetics.org/lookup/suppl/doi:10.1534/genetics.114.167445/-/DC1.
[1]Corresponding authors: Biology Department, Gettysburg College, 300 N. Washington St., Gettysburg, PA 17325. E-mail: sjames@gettysburg.edu; Millsaps College, 1701 N. State St., Jackson, MS 39210. E-mail: mcguisl@millsaps.edu

nuclear pores and may equilibrate across the nuclear envelope (De Souza *et al.* 2004). In *A. nidulans*, the activity and proper localization of three protein kinases are required for initiation of mitosis: the CDK1/CYCLINB protein kinase complex ($NIMX^{CDC2}$/$NIME^{CYCLINB}$), the NIMA kinase, and a polo-like kinase (PLKA), all three of which must be inactivated to allow mitotic exit (Bachewich *et al.* 2005; Osmani *et al.* 2006). The activity of CDK1/CYCLINB is tightly regulated by phosphorylation and is part of an autocatalytic feedback loop (Ye *et al.* 1995); its activity is inhibited by the $ANKA^{WEE1}$ kinase and activated by the $NIMT^{CDC25}$ phosphatase. Furthermore, active NIMA kinase is required for mitotic initiation; in the absence of functional NIMA kinase, cells with fully active CDK1/CYCLINB arrest in late G2 (Osmani *et al.* 1991). NIMA activity is also regulated by phosphorylation (Ye *et al.* 1995) and is required for proper localization of CDK1/CYCLINB (Wu *et al.* 1998) and tubulin (Ovechkina *et al.* 2003) into the nucleus at the G2/M transition. Specifically, the $SONA^{GLE2}$ and $SONB^{NUP98}$ nucleoporins interact with NIMA to regulate the nuclear localization of $NIMX^{CDC2}$/$NIME^{CYCLINB}$ (Wu *et al.* 1998; De Souza and Osmani 2009). Wu *et al.* (1998) demonstrated that $NIMX^{CDC2}$ colocalizes in the nucleus with $NIME^{CYCLINB}$ during S and G2, that the G2 arrest that occurs in the absence of NIMA activity occurs with predominantly cytoplasmic $NIMX^{CDC2}$/$NIME^{CYCLINB}$, and that in *nimA1* mutants the *sonA1* suppressor of *nimA1* re-establishes nuclear localization of $NIMX^{CDC2}$/$NIME^{CYCLINB}$ and entry into mitosis. These data provide evidence that proper localization of $NIMX^{CDC2}$/$NIME^{CYCLINB}$ is both regulated and essential for controlling mitotic entry during the partially closed mitosis of *A. nidulans*.

CDK1 localization and cell cycle progression depend upon the localization of CYCLINB (Nigg 1995). $NIME^{CYCLINB}$ localization has been characterized through the cell cycle in *A. nidulans* (Wu *et al.* 1998; De Souza *et al.* 2009); its nuclear localization is closely mirrored by $NIMX^{CDC2}$ localization (Nayak *et al.* 2010). $NIMX^{CDC2}$ and $NIME^{CYCLINB}$ become visible in the nucleus at or near the G1/S boundary and disappear from the nucleus during mitosis. De Souza *et al.* (2009) localized $NIME^{CYCLINB}$ in live cells to the nucleoplasm and to the spindle pole bodies (SPBs) during interphase and early mitosis; this work demonstrated that the partial disassembly of the nuclear pore complex (NPC) at mitotic prophase allows most of the $NIME^{CYCLINB}$ to exit the nucleus; however, a nuclear pool remains, concentrated at the SPBs and also in the region of the segregating kinetochores. It is to this pool of $NIME^{CYCLINB}$ that $NIMX^{CDC2}$ presumably remains bound. The nuclear $NIME^{CYCLINB}$ disappears sequentially during mitotic progression. The SPB pool disappears during anaphase, followed rapidly by the pool at the kinetochores. Surprisingly, $NIMX^{CDC2}$ exits the nucleus slightly before the complete destruction of nuclear $NIME^{CYCLINB}$ (Nayak *et al.* 2010).

While phosphorylation/dephosphorylation and cell cycle-regulated localization of mitotic proteins have been shown to play integral roles in controlling the transition from G2 into mitosis in *A. nidulans*, much remains to be learned. $NIMX^{CDC2}$ encodes the only known $p34^{CDC2}$ protein kinase in *A. nidulans*, and its activity is required at both G1 and G2 (Osmani *et al.* 1994). $NIME^{CYCLINB}$ also functions at both G1 and G2 in *A. nidulans*. While *nimE6* causes a G2 arrest at restrictive temperature (O'Connell *et al.* 1992), the *nimE10* mutation (originally identified as *nimG*10) arrests cells in S at restrictive temperature (Supporting Information, Figure S1). The G1-specific functions of $NIMX^{CDC2}$/$NIME^{CYCLINB}$ are not well understood. To better understand cell cycle regulation in *A. nidulans* by $NIMX^{CDC2}$/$NIME^{CYCLINB}$, an extragenic suppressor screen to identify genes that interact with $NIMX^{CDC2}$ was undertaken (McGuire *et al.* 2000). The *snxA1* mutation was identified in this screen as an extragenic suppressor of $nimX2^{F223L}$. *snxA1* suppresses the *nimX2* heat-sensitive G2 arrest, allowing cells to enter and exit mitosis at the restrictive temperature for *nimX2*; additionally, and independent of its suppression of *nimX2*, *snxA1* confers cold sensitivity, leading to a G1 arrest at its restrictive temperature (McGuire *et al.* 2000). Thus, as is the case for $nimX^{cdc2}$ and $nimE^{cyclinB}$ mutations, the *snxA1* mutation has effects on the cell cycle at both G1 and G2. In this article, we report genetic, cytological, and molecular analysis of *snxA* and demonstrate that it encodes the *A. nidulans* homolog of *Saccharomyces cerevisiae* Hrb1/Gbp2 proteins.

Hrb1/Gbp2 and the more divergent but similar protein Npl3 are nonessential shuttling messenger RNA (mRNA)-binding proteins that are similar to members of the mammalian serine-arginine-rich (SR) protein family (Rougemaille *et al.* 2008). SR proteins are a class of small nuclear ribonucleoprotein splicing factors that harbor two distinct types of domains: RNA recognition motifs (RRMs), responsible for RNA binding, and SR domains, long repeats of serine-arginine or arginine/serine dipeptides that are extensively phosphorylated (Ma and Poon 2011). Some RRM proteins contain RGG/RG tripeptide motifs that serve as sites for arginine methylation (Thandapani *et al.* 2013). In addition to their functions in spliceosome assembly and catalysis (Sanford *et al.* 2004), SR proteins are also involved in mRNA transcription and export (TREX) (reviewed in Reed and Cheng 2005; Rougemaille *et al.* 2008).

In budding yeast, Hrb1/Gbp2 are recruited to and associate cotranscriptionally with mRNA transcripts by physical association with the TREX complex and Ctk1, a member of the cyclin-dependent kinase family that is the catalytic domain of C-terminal domain kinase 1 (Ctdk-1) (Figure S2). Ctdk-1 is a protein kinase required for efficient transcription elongation that phosphorylates the C-terminal domain of RNA polymerase II (RNAPII) (Hurt *et al.* 2004). The TREX complex consists of the THO complex (composed of Tho2, Hpr1, Mft1, and Thp2), which associates with RNA polymerase II as it transcribes, and Sub2 and Yra1, export factors that bind to THO and function as a platform to recruit Hrb1/Gbp2 (Hurt *et al.* 2004). Hrb1/Gbp2 associate both with the genes and the growing, unprocessed mRNA transcripts produced from them and remain bound to the mRNA transcripts as part of the messenger RNA–protein complex (mRNP). As shuttling proteins, Hrb1/Gbp2 remain bound to the transcript during export from the nucleus; they also remain associated with the mRNP during

translation (Windgassen *et al.* 2004). Nuclear export of the mRNP requires the THO complex (Hacker and Krebber 2004) and the Mex67-Mtr2 dimer, an export receptor that interacts with nucleoporins (Strasser and Hurt 2000). Yra1 interacts with Mex67 (Strasser and Hurt 2000) and is essential for mRNA export for some, but not all, transcripts (Kim Guisbert *et al.* 2005). In addition to their functions in mRNA transcription and export, SR-like proteins act as localization signals that aid in delivering the mRNP to the translational machinery (Windgassen *et al.* 2004). More recently, both Hrb1 and Gbp2 have been shown to associate with the budding yeast spliceosome (Warkocki *et al.* 2009), with unspliced transcripts close to 5′ intron sequences (Tuck and Tollervey 2013), and with intron sequences and splicing factors (Hackmann *et al.* 2014).

While Hrb1/Gbp2 remain bound to transcripts during translation, localization studies show that Hrb1 is predominantly nuclear at steady state and that its re-import into the nucleus is mediated by the Mtr10 karyopherin import receptor (Hacker and Krebber 2004). Both Hrb1 and Gbp2 are phosphorylated by the cytoplasmic SR-specific protein kinase Sky1 (Porat *et al.* 2006; Ma and Poon 2011). This phosphorylation increases the affinity of Hrb1 for the mRNP. However, while Sky1 phosphorylation is required for re-entry of Gbp2 into the nucleus, it is not essential for nuclear import of Hrb1.

Hrb1/Gbp2 appear to have roles in mRNA export; however, deletion of these genes does not disrupt or alter the nucleocytoplasmic distribution of bulk polyadenylated mRNAs (Hacker and Krebber 2004). Interestingly, overexpression of Gbp2 leads to a delay in G1 (Stevenson *et al.* 2001). As suggested by Rougemaille *et al.* (2008), Hrb1/Gbp2 may act as dedicated adaptors that recognize specific sets of transcripts. Hackmann *et al.* (2014) recently demonstrated that Hrb1/Gbp2 function both to recognize and to mediate the elimination of aberrantly spliced transcripts via binding to Mtr4 and to mediate the nuclear export of correctly spliced transcripts via Mex67 (Hackmann *et al.* 2014).

Given that the *A. nidulans* Hrb1 homolog, *snxA*, was identified as a genetic interactor with $nimX^{cdc2}$ and that the *snxA1* mutation arrests cells in G1 at its restrictive temperature, it is possible that $SNXA^{HRB1}$ interacts with cell cycle-specific transcripts or proteins. The SR/RRM family has not previously been implicated in the regulation of the G2/M transition. These findings may therefore represent a novel regulatory mechanism in cell cycle control of *A. nidulans*.

Materials and Methods

Strains and general techniques

Strains used in this study are listed in Table S1. PCR primers used for gene deletion, gene tagging, and molecular diagnoses are shown in Table S2. Phusion Polymerase was used for all PCR experiments, and all other DNA-modifying enzymes were from New England BioLabs. Standard methods of *Aspergillus* culture (Kafer 1977), genetic analysis (Pontecorvo *et al.* 1953; Kaminskyj 2001), construction and analysis of heterokaryons and diploids (Todd *et al.* 2007), and *Aspergillus* transformation (Ballance *et al.* 1983) were employed. Appropriately supplemented minimal media (1% glucose) were used for all strain construction and genetic mapping. Rich media, composed of minimal medium (Kafer 1977) supplemented with 0.5% yeast extract and containing 2% glucose, were used for kinase assay experiments and to grow cells for DNA-mediated transformation.

Generation of a new snxA allele by a noncomplementation screen

To generate a new *snxA* allele, we mutagenized a diploid strain, dSWJ 3693, homozygous for *nimX2* and heterozygous for *snxA1* (*riboA*1/+ +/*yA2*; *nimX2 snxA1 wA*2/*nimX2* + +; +/*pyroA4*; +/*methB3*; *nicB8*/+), in which the *snxA1* chromosome is marked by the *wA*2 white-spored mutation. This diploid is green because it carries a wild-type *wA* allele and it expresses the *nimX2* temperature-sensitive (TS) lethality at 39°–44°. Freshly harvested conidia (2×10^7) were treated for 30 min at 30° with 0.8 or 1.2 μg/ml of the UV-mimetic 4-nitroquinoline-1-oxide (4-NQO), inactivated by treatment with 10% $Na_2S_2O_3$ for 5 min, and washed twice in dH_2O, and then 5×10^6 spores were spread on appropriately supplemented minimal medium and grown for 4–6 days at 41° to select for strains that gain the ability to grow at the *nimX2* restrictive temperature. Because one copy of *snxA* is defective, we reasoned that new *nimX2*-suppressing mutations might occur in the remaining wild-type *snxA* allele. Alternatively, suppression may occur by back mutation or reversion in a *nimX2* allele or by dominant mutations in genes other than *nimX* or *snxA*. Thirteen candidate TS+ green colonies were recovered, streaked three times, and grown at 37° to ensure clonal purity.

To recover the new mutations in a haploid background, a parasexual genetic approach was employed (Todd *et al.* 2007) to break down the diploid strains into their component haploid strains nonmeiotically, *i.e.*, via random assortment of chromosomes without crossing over. Each TS+ strain was streaked in a line on rich media containing the microtubule-destabilizing agent benomyl (Bonide, Trainor and Bonide Products, Inc.) at 60, 67.5, 75, and 82.5 μg/ml and grown at 33° for 8 days until haploid sectors grew out. Haploids were distinguished from diploids by segregation of yellow (*yA*2 on chromosome I) or white (*nimX2 snxA1 wA*2 on chromosome II) sectors or by occasional green sectors from the green diploid parent. Thirty-five white, yellow, or green haploid sectors were recovered from each TS+ diploid and streaked three times to clonal purity. The haploids were then screened on minimal media for the auxotrophic markers (*pyroA*4, *nicB*8, *methB*3, *riboA*1) and for temperature sensitivity. As expected, all *wA*2 sectors were phenotypically *nimX2 snxA1*. Among the TS+ candidate diploids, representative yellow and green haploids derived from 7 of these 13 strains were analyzed further, as reported in *Results* (below).

Fluorescence microscopy

For fluorescence microscopy, cells were grown in minimal media containing 1% glucose or 50 mM glycerol as the carbon source. To visualize fluorescently labeled proteins, conidia were incubated on coverslips as described (Harris *et al.* 1994) and fixed for 20 min in PEMF (80 mM PIPES, 1 mM EGTA, 1 mM $MgCl_2$, 4% formalin). Nuclear staining with 2,4-diamidino-2-phenylindole (DAPI) following fixation was as described (Brody *et al.* 1991). Experiments were performed in duplicate; 200 germlings (containing fewer than eight nuclei/germling) per replicate were visualized and quantitated using a Zeiss Axioimager.M1 microscope equipped with a Photometrics Coolsnap HQ^2 camera. Exit from mitosis was determined by dissolution of the mitotic spindle in strains harboring both GFP-α-tubulin and SNXA::mRFP. For $NIME^{CYCLINB}$ localization experiments, bulk localization of $NIME^{CYCLINB}$ was quantitated; detecting the localization of the small nuclear pool that remains after mitotic entry and is degraded at mitotic exit is beyond the capabilities of our instrumentation.

snxA gene deletion, overexpression, and gene tagging

snxA-predicted gene structure is complex, with as many as 11 coding exons and in which the first 2 exons are very short: the first exon = 34 nt, containing 30 nt of 5′ UTR and 1 1/3 codons, ATGG; and the second exon = 16 nt and encodes 5 1/3 codons [*Aspergillus* Comparative Sequencing Project, Broad Institute of Harvard and MIT (http://www.broadinstitute.org/)]. Furthermore, these short ORFs are interspersed with unusually long and GC-rich introns of 766 and 548 nt, respectively. Moreover, an alternative start codon, 42 nt inside the 3′ end of the second intron and in-frame with the third exon, would eliminate the first 2 short exons and would create a 9-exon protein that differs by ^{13}N-terminal amino acids from the 11-exon protein.

By one-step gene replacement, *snxA* was deleted by replacing all but the first two short exons and by completely eliminating the alternative nine-exon gene. Three-way fusion PCR was used to create a linear deletion construct (Yu *et al.* 2004) (Table S2) using the *Aspergillus fumigatus pyroA* gene as a selectable marker, followed by nested PCR to amplify a sufficient amount of purified product for DNA-mediated transformation. This nested construct was introduced into a *snxA*+ host strain (tSWJ 2973: *pyrG*89; *pyroA*4 Kutr-L::*pyrG* Af; *nicA*2; *riboB*2) in which the nonhomologous end-joining pathway of DNA repair (*nkuA* gene, encoding Ku70) was transiently disrupted (Nielsen *et al.* 2008) to facilitate homologous integration (Nayak *et al.* 2006). Weakly growing *pyroA*+ transformants were selected at 37° for 6 days, followed by serial streaking to clonal purity. The expected patterns for gene replacement at the *snxA* locus were observed by Southern blotting (data not shown), and two of these deletions were further verified by *trans*-locus PCR using primers that lie outside of the region covered by the nested deletion construct (Figure S3).

Overexpression studies were performed with strains carrying one copy of an *alcA*-driven *snxA* allele integrated at the *argB* locus. The *alcA*::*snxA* construct was made by amplifying the alternative nine-exon gene from genomic DNA, using PCR primers into which a novel *Spe*I or *Bam*HI restriction site was incorporated (Table S2). The 2249-nt genomic PCR clone was digested first with *Spe*I, blunted by treatment with Klenow fragment, and then digested with *Bam*HI. This fragment was cloned into the *Sma*I and *Bam*HI sites of the plasmid pSDW194 (James *et al.* 1999) that contains the inducible-repressible *A. nidulans alcA* alcohol dehydrogenase gene promoter (Waring *et al.* 1989) and the *A. nidulans argB* gene as a selectable marker. Southern blotting with probes against *argB* and *snxA* was used to diagnose single *argB* integrations (Figure S4). *alcA*::*snxA* expression was strongly induced in minimal medium containing 200 mM ethanol + 0.04% fructose as the carbon source. Basal expression was achieved using 50 mM glycerol, and *alcA*::*snxA* expression was repressed on rich media containing 2% glucose.

GFP and mRFP tags were added to the C terminus of the wild-type *snxA* gene by using universal tagging cassettes (Yang *et al.* 2004). Linear tagging constructs were generated by three-way fusion PCR (Table S2), followed by nested PCR. These constructs were transformed into a *snxA*+ host (tSWJ 2353: *pyrG*89; *pyroA*4 Δ*nkuA*::*argB*; *nimO18*; *riboB*2). From each transformation five *pyrG*+ transformants were recovered and streaked three times to clonal purity. Creation of *snxA*::GFP and *snxA*::mRFP was verified in all 10 *pyrG*+ strains by *trans*-locus PCR (data not shown). Several of these strains were examined by fluorescence microscopy; all produced strong nuclear signals in interphase cells. These strains were outcrossed to remove the *nimO18* mutation and to combine the tagged alleles with other relevant markers and mutations, including GFP-α-tubulin, GFP-$nimE^{cyclinB}$, $nimX2^{cdc2}$, $nimT23^{cdc25}$, and $nimE6^{cyclinB}$.

A myc9 epitope tag was added to the C terminus of *snxA* wild-type, *snxA1*, and *snxA2* alleles by using universal tagging cassettes. This tag contains an 11-amino-acid GAGAGAGFDGA N-terminal linker followed by the myc 10-amino-acid repeats; each myc repeat is flanked by a GA dipeptide. The myc9 tag was generated *de novo* using two self-dimerizing primers as described by Nakajima and Yaoita (1997) (Table S2). The primers were 5′ phosphorylated using T4 Polynucleotide Kinase (New England BioLabs), boiled 3 min to inactivate the kinase and then used as template to amplify myc tags of varying length via 30 cycles of PCR. AmpliTaq DNA Polymerase Stoffel fragment (Applied Biosystems) was used for amplification in 1× Stoffel Buffer with annealing temperature 62° and a 10-min extension at 72°. The largest PCR products were recovered and purified (QIAEX II Gel Extraction Kit, QIAGEN), cloned into the *Eco*RV site of pBluescript KS(+), and sequenced. One of these clones, containing a myc9 fragment, was amplified further to add, at the 5′ end, a *Bsp*DI site followed by an N-terminal GAGAGAGFDGA linker; to the 3′ end, a stop codon followed by a *Hin*dIII site were added (Table S2). This amplicon was cloned into the *Bsp*DI and *Hin*dIII sites of pBluescript KS(+) and then sequenced to verify the $(GA)_3$GFDGA-myc9-STOP tag. Finally, three universal myc9-tagging cassettes were

constructed by cloning in the *pyrG*, *pyroA*, or *riboB* selectable marker genes from *A. fumigatus*. *pyrG*^{Af} was removed from a plasmid, pCLS366, as an *Eco*RV–*Eco*RI fragment and cloned into the corresponding sites in the myc9 plasmid to generate p*myc9-pyrG*^{Af}. *pyroA*^{Af} and *riboB*^{Af} were removed from pTN01 and pTN02, respectively (Nayak *et al.* 2006), as *Hin*dIII (blunt)–*Pst*I fragments and cloned into the *Eco*RV and *Pst*I sites of the myc9 plasmid to create p*myc9-pyroA*^{Af} and p*myc9-riboB*^{Af} (Figure S5).

Using three-way fusion PCR followed by one-step gene replacement, the *snxA*+, *snxA1*, and *snxA2* genomic loci were C-terminally tagged with *myc9*::*riboB*^{Af} (Table S2) in five *A. nidulans* host strains (*snxA*+: tSWJ 2888; *snxA1*: tSWJ 5573/5574; *snxA2*: tSWJ 5583/5584) and diagnosed by *trans*-locus PCR (data not shown).

Isolation and characterization of snxA complementary DNAs

A 1.3-kb PCR fragment corresponding to the AN3739 *snxA*-predicted coding region (spanning exons 6–11) was used to screen an *A. nidulans* λgt10 complementary DNA (cDNA) library (generously provided by S. Osmani) (Osmani *et al.* 1988). Of eight independent phage isolates that were amplified and cloned into pBSKS(+), four were judged to be full-length based on their size (1.8–2.1 kb). Sequencing revealed two alternative *snxA* cDNAs (two clones of each) that were spliced differently at their N termini and composed of either 9 or 11 exons (Figure S6). Both of these isoforms correspond to alternatively spliced AN3739 transcripts identified previously by EST sequencing of *A. nidulans* cDNA libraries [*Aspergillus* Comparative Sequencing Project, Broad Institute of Harvard and MIT (http://www.broadinstitute.org/)] and as described above. To assess their functions, the cDNAs were fused with the *A. nidulans alcA* promoter in plasmid pSDW194 (James *et al.* 1999). Following transformation of *snxA1* mutants SWJ 3676 and SWJ 3678, Southern blotting was used to identify strains carrying a single copy of *alcA*-driven *snxA* integrated at the *argB* or *snxA* loci. Ability to complement *snxA1* cold sensitivity was assessed on inducing medium (200 mM ethanol + 0.04% fructose), on medium that allows basal expression (50 mM glycerol), and on repressing medium (2% glucose).

mRNA transcript analysis

RNA isolation and gene expression were determined for wild-type (PCS 439), *snxA1* (SWJ 4030), and *snxA2* (SWJ 5562) strains using quantitative RT-PCR (qRT-PCR) as described (Alam *et al.* 2012). Randomly cycling vegetative mycelia grown at 32° were collected by vacuum filtration using Miracloth (Calbiochem), frozen in liquid nitrogen, and lyophilized overnight. Total RNA was extracted using an RNeasy plant kit (Qiagen) per manufacturer's instructions. RNA concentration and RNA quality were determined using a NanoDrop spectrophotometer to determine 260/280 ratio, followed by native agarose gel electrophoresis. Total RNA was diluted to 400 ng/μl, and genomic DNA (gDNA) elimination and reverse transcription were performed using a QuaniTect reverse transcription kit (Qiagen) according to manufacturer's instructions, including no reverse transcriptase controls. Samples were diluted 1:5 and Quantitative real-time PCR (qPCR) was performed using iQ SYBR Green Supermix (Qiagen) according to the manufacturer's instructions. Appropriate negative controls were used in all experiments (no template DNA; no reverse transcriptase) for each gene. Six replicates of each reaction were performed using a 20-μl total volume in 96-well optical plates in a C1000 thermal cycler using a CFX96 real-time detection system (Bio-Rad). *actA* (actin) was used as the reference gene, using primers actF and actR that amplify across an intron; for *snxA*, either of two forward primers, one straddling intron 9 (snxA-q1) and one in exon 10 (snxA-q2), was paired with one reverse primer (snxA-q3), located 80 nt into exon 11 (Table S2). qPCR amplification conditions were the following: 95°/3 min for one cycle, 95°/15 sec, 60°/15 sec, 72°/20 sec for 44 cycles, 95°/10 sec. Melt curve analysis was performed starting at 65° and rising by increments of 0.5° every 5 sec to 95°. Expression was normalized to *act*A and calculated using the ΔΔCt method (Livak and Schmittgen 2001). Five independent replicate experiments were performed with nearly identical results.

Western blot analysis and kinase assays

Protein purification, Western analysis, and kinase assays were performed as previously described (Osmani *et al.* 1991; Liu *et al.* 2010). Briefly, total protein extracts were generated from lyophilized mycelia as described (Liu *et al.* 2010). For NIMX detection, 100 μg of extracts were separated by SDS-PAGE, blotted to nitrocellulose, and probed with anti-NIMX E77 antibody (kind gift of Stephen Osmani). Detection was performed using goat anti-mouse IgG, HRP conjugate (Millipore; #12-349), and GE Healthcare Advance Chemiluminescent Western blotting detection kit. For the histone ^{1}H kinase assay (described in Osmani *et al.* 1991), anti-NIMX E77 antibody was incubated with 200 μg of extracts, and immune complexes were precipitated with protein A/G sepharose (Pierce). Following precipitation, beads were washed four times and then resuspended in 20 μl kinase assay buffer (Osmani *et al.* 1991), incubated with substrate (Millipore histone ^{1}H; #14-155) for 5 min, and the reaction was stopped by addition of 20 μl Laemmli sample buffer. After boiling for 5 min, the entire supernatant for each reaction was separated by SDS-PAGE, and the dried gel was exposed to autoradiography film.

For SNXA detection, 2.5 μg of extracts were separated by SDS-PAGE (4–20% TBX gels, Bio-Rad), blotted to PVDF, and probed with either myc.A7 mouse mAb at 1:3000 (Abcam ab18185) or DM1A anti-α-tubulin mouse mAb at 1:1000 (Abcam DM1A) followed by 1:5000 anti-mouse IgG HRP (Promega W4021). Protein complexes were detected by a 1-min exposure in 5 ml of TMB stabilized substrate for HRP (Promega W4121). For GFP-NIME^{CYCLINB} detection, 2.5 μg of extracts was separated by SDS-PAGE (10% Tris-glycine gels, Bio-Rad), blotted to nitrocellulose, and probed with anti-GFP antibody at 1:1000 (Invitrogen A11122) followed

by 1:10,000 anti-rabbit IgG HRP (Santa Cruz Biotechnology Sc-2004). The blots were stripped and reprobed with anti-α-tubulin mouse mAb at 1:1000 (Sigma T9026) followed by 1:10,000 anti-mouse HRP (Pierce 32230).

Results

snxA interacts with the CDK1 mitotic regulatory pathway

To determine if the *snxA1* mutation is allele specific, *snxA1/nimX* double mutants were generated with three heat-sensitive *nimX* alleles (*nimX1*^{G225S}, *nimX2*^{F223L}, and *nimX3*^{Y306H}); colony growth at increasing temperatures was compared for single mutants and double mutants (Figure 1). The *snxA1* mutation conferred cold sensitivity at 20° and reduced colony size at permissive and semipermissive temperatures (25°–43°) in all strains tested. Suppression of heat sensitivity was evident in all three double-mutant strains at 37° and for *snxA1/nimX1* and *snxA1/nimX2* double mutants at 43°.

snxA1 double mutants were generated with four additional heat-sensitive G2-arresting mutations [*nimE6*^{cyclinB}, *nimT23*^{cdc25}, and *nimA1/nimA5* (O'Connell *et al.* 1992)], two S-phase-arresting *nim* mutations [*nimE10*^{cyclinB} (Figure S1) and *nimP22*$^{DNApol\varepsilon}$ (S. James, unpublished results)], and two late G1-arresting mutations [*nimO18*^{dbf4} (James *et al.* 1999) and *nimQ20*^{mcm2} (James *et al.* 1995)]. The late-G1-arresting *nimO18*^{dbf4} and *nimQ20*^{mcm2} mutations fail to initiate DNA synthesis at restrictive temperature. However, they do undergo mitotic catastrophe by attempting to segregate their unreplicated chromatin; *i.e.*, they undergo a pseudomitosis resulting from failure to activate a DNA replication checkpoint at the G1/S transition (James *et al.* 1999). Thus, these mutants are presumed to activate the CDK1 mitotic induction pathway at restrictive temperature. Growth of double mutants was compared to single mutants at increasing temperatures (Figure 2 and Figure 3). *snxA1* suppressed the heat-sensitive G2-arrest phenotypes of *nimX2*^{cdc2}, *nimE6*^{cyclinB}, and *nimT23*^{cdc25} at 37° and 43° (Figure 2A). In contrast, *snxA1* failed to suppress the *nimA1* and *nimA5* G2-M regulatory defects, and instead the double mutants were more growth-impaired than either single mutant at the permissive temperatures of 29° and 33° (Figure 2B). Similarly, *snxA1* exhibited little or no suppression of the *nimE10*^{cyclinB} and *nimP22*$^{DNApol\varepsilon}$ S defects, and *snxA1* failed to suppress the heat-sensitive G1 arrest of *nimO18*^{dbf4} and *nimQ20*^{mcm2}. Instead, and contrasting with *snxA1* rescue of CDK1 pathway mutations, growth and temperature defects became more severe in these latter four *snxA1* double mutants, as expected for mutations that operate in unrelated pathways. Therefore, *snxA1* suppression of heat-sensitive cell cycle defects appears restricted to components of the CDK1 mitotic regulatory pathway. Both NIME^{CYCLINB} and NIMT^{CDC25} are specifically required for the activation of NIMX^{CDC2} to allow mitotic entry, and NIMA is required for the partial disassembly of nuclear pore complexes, which allows entry of the active NIMX$^{CDC2/CYCLINB}$ complex into the nucleus (De Souza *et al.* 2003, 2004). The suppression of three different *nimX*^{cdc2} alleles and of mutations in multiple activators of the NIMX^{CDC2}/NIME^{CYCLINB} G2-M regulatory pathway, but not of mutations affecting G1- or S-phase control or the NIMA G2-M regulator, strongly suggests a role for SNXA in the regulation of the G2/M transition via the CDC2/CYCLINB regulatory pathway.

SNXA encodes the A. nidulans homolog of Hrb1^{Sc}/Gbp2^{Sc} and human heterogeneous ribonucleoprotein-M

snxA (***s***uppressor-of-***n***im***X***^{cdc2}) was previously assigned to linkage group II (LGII) via parasexual mapping (McGuire *et al.* 2000). After several unsuccessful attempts to complement *snxA1* using a LGII-specific cosmid library (Brody *et al.* 1991) [obtained from the Fungal Genetics Stock Center (FGSC), Kansas City, MO] or a total genomic library (Osherov and May 2000) (obtained from the FGSC), the location of *snxA* within LGII was determined by linkage analysis. The initial discovery of linkage to *anB8* (17.4 map units, $n = 144$) was followed by three-factor crosses involving *snxA1*, *cnxE16*, and *hisG113*, in which *snxA* localized 10.7 map units rightward of *cnxE* and 1.3 map units rightward of *hisG* ($n = 224$).

To isolate the wild-type *snxA* gene, a group of five overlapping fosmids (Galagan *et al.* 2005) (obtained from the FGSC) that span the relevant region were cotransformed into a *snxA1 argB*2 strain (SWJ 3676: *riboA1*; *snxA1*; *argB2*; *pyroA4*; *chaA1*) using the *A. nidulans* autonomously replicating helper plasmid pDHG25 (Brody *et al.* 1991) (obtained from the FGSC), which carries *A. nidulans argB* as a selectable marker. Cotransformed cells were grown for 18 hr at 37° to establish thousands of *argB*+ transformants, then shifted to 20° for 8 days to select for complementation of *snxA1* cold sensitivity. Only one fosmid, 8201-D10, complemented *snxA1*; >100 *snxA*+ *argB*+ cotransformants were obtained. 8201-D10 overlapped a noncomplementing fosmid (8199-G2) over two-thirds of its length, thereby eliminating 10 of 16 fosmid-borne genes from further consideration and narrowing the search to a group of 5 protein-coding genes (AN3738 to AN3742) and one leucyl-transfer RNA (tRNA) in the non-overlapping region of 8201-D10. Four fragments covering this region were subcloned into pBluescript KS(+) and transformed into a *snxA1* strain. Only one plasmid, containing AN3739 and lacking the tRNA gene, complemented *snxA1*, thus identifying AN3739 as the putative *snxA* gene.

Deletion of AN3739/*snxA* was accomplished by one-step gene replacement (Figure S3). *ΔsnxA* strains were viable and slightly more impaired than *snxA1* for vegetative growth and conidiation at all temperatures. Deletion of *snxA* phenocopied the *snxA1* mutation, conferring cold-sensitive lethality at 20°, mild heat sensitivity at 43°, and suppressing the heat sensitivity of *nimX1* and *nimX2* at 37° and 43° (Figure 4A). Conversely, and similar to *snxA1 nimA5* and *snxA1 nimA1* double mutants (Figure 2B), *ΔsnxA* did not suppress *nimA5* (Figure 4B); these double mutants remained heat sensitive and cold sensitive, with pronounced impairment of growth

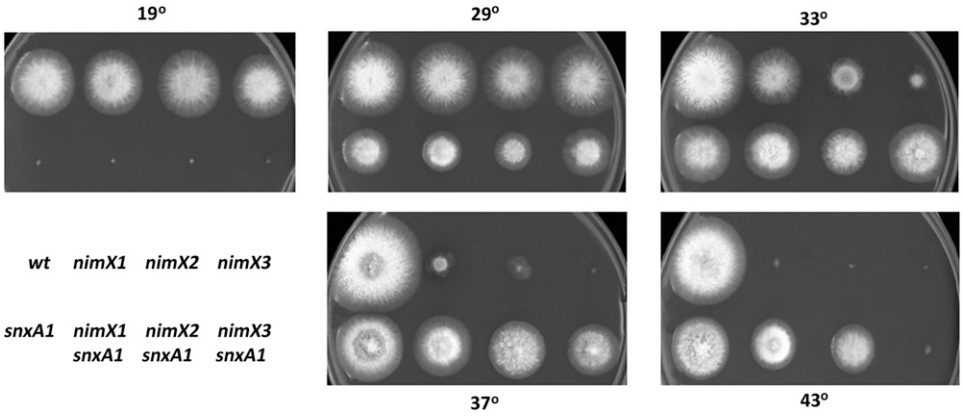

Figure 1 *snxA1* suppresses multiple alleles of *nimX*^{cdc2}. Growth phenotypes of single and double mutants on minimal medium at the indicated temperatures. Days of growth at each temperature are as follows: 19°, 6 days; 29°/33°/37°/43°, 2.5 days.

and conidiation at the permissive temperatures of 29° and 33°, typical of mutations that act through different pathways.

A noncomplementation screen was used to generate an additional *snxA* mutation in a diploid strain homozygous for *nimX2* and heterozygous for *snxA1*, as described in *Materials and Methods*. Thirteen diploid revertants that had regained the ability to grow at the *nimX2* restrictive temperature of 41° were haploidized by treatment with benomyl. Haploid strains derived from 7 of the 13 candidates were crossed to *hisG113*, and of these one harbored a cold-sensitive *nimX2* suppressor that was tightly linked to *hisG* (two recombinants in 60 progeny, 3.3 map units). This mutant was named *snxA2*. To verify the ability of *snxA2* to suppress *nimX2*, *snxA2 nimX2* double mutants were resynthesized by crossing *snxA2 nimX*+ × *nimX2 snxA*+. In these double mutants, *snxA2* suppressed *nimX2* temperature sensitivity at 37° and 43° in a manner similar to *snxA1* (Figure S7). The *snxA2* phenotype differs from *snxA1*. Whereas *snxA1* grows optimally and conidiates strongly at 37°, *snxA2* mutants grow and conidiate optimally at 33° and exhibit a defect in conidiation at 37°, suggesting that *snxA2* harbors a more severe defect than *snxA1* and that *snxA1* and *snxA2* result from different alterations (Figure 5).

To verify the location of the *snxAl* and *snxA2* mutations, one PCR-derived and two plasmid-derived linear wild-type DNA fragments were used to complement *snxA1* in two strains (tSWJ 5573/5574) and *snxA2* in two strains (tSWJ 5567/5584). These strains harbored a deletion of the *nkuA* (Ku70) gene to facilitate targeted integration by homologous recombination (Nayak *et al.* 2006). Each of these transformations yielded hundreds of transformants that efficiently complemented the cold sensitivity of the mutants (Figure 6). The shortest linear DNA, a 3353-nt *Eco*RI–*Sna*BI fragment, begins approximately in the middle of intron 1 and encompasses exons 2–11 and 90% of the AN3739 3′ UTR (263 of 291 nt).

Allelism between *snxA1*, *snxA2*, and *ΔsnxA* was assessed in complementation tests using diploids and heterokaryons (Figure S8). In heterozygous diploids, each *snxA* mutant was fully recessive (Figure S8A). Only one homozygous diploid, *snxA1/snxA1*, was isolated (Figure S8A). Although balanced heterokaryons harboring *ΔsnxA/snxA1* and *ΔsnxA/snxA2* were repeatedly established, diploids could not be derived after three independent attempts. Therefore, complementation was examined in these balanced heterokaryons (Figure S8B). *snxA1* and *snxA2* failed to complement *ΔsnxA*, conferring cold-sensitive lethality at 20° and growth impairment at 43° similar to haploid *snxA* mutants. Interestingly, at 43° the growth defect of *ΔsnxA/snxA2* heterokaryons was dramatically enhanced, showing greater impairment than *ΔsnxA/snxA1* heterokaryons or haploid *ΔsnxA* and *snxA2* single mutants.

AN3739 shares ~30% identity with *S. cerevisiae* Hrb1/Gbp2 ($1e^{-45}$ and $2e^{-43}$, respectively), nonessential shuttling mRNA-binding proteins containing an N-terminal SR domain and three RRMs (Figure S6A). As the only Hrb1/Gbp2-homologous protein in the *A. nidulans* genome, AN3739 contains a similar overall structure, with three highly conserved RRMs and an N-terminal SR domain that is slightly more similar to Hrb1 than to Gbp2 (34 identities/eight similarities *vs.* 33 identities/four similarities). The closest human homolog of AN3739, heterogeneous ribonucleoprotein-M (hnRNP-M, $3e^{-27}$), is an abundant spliceosomal component involved in pre-mRNA splicing and alternative splicing (Lleres *et al.* 2010; Xu *et al.* 2014). hnRNP-M also contains three conserved RRM motifs but lacks an N-terminal SR domain (Figure S6B). SNXA and hnRNP-M share two features that distinguish them from the budding yeast proteins. First, the sequences between RRM1-RRM2 and RRM2-RRM3 are glycine-rich, containing several runs of between two and seven glycines. Second, SNXA and hnRNP-M contain tripeptide motifs that are commonly methylated on arginine. SNXA contains seven RGG tripeptides, of which five are clustered between RRM2 and RRM3; hnRNP-M has undergone an expansion of this same region, which contains 25 RMG/RVG/RIG/RMA/RMV motifs that are known to be methylated (Hung *et al.* 2009).

snxA function was examined further by overexpressing genomic and cDNA clones. Overexpression of a 9-exon wild-type AN3739/*snxA* genomic DNA, containing exons 3–11 and 90% of the 3′ UTR, efficiently rescued *snxA1* cold sensitivity and abrogated the suppression of *nimX2* by *snxA1* (Figure S4C; Figure S9). In addition, overexpression of this *alcA*::*snxA*+ gDNA complemented *ΔsnxA* defects in growth and cold sensitivity (Figure S10). Unexpectedly, overexpression of the 9-exon region obtained from *snxA1* mutant gDNA also complemented *snxA1* efficiently (data not shown), suggesting

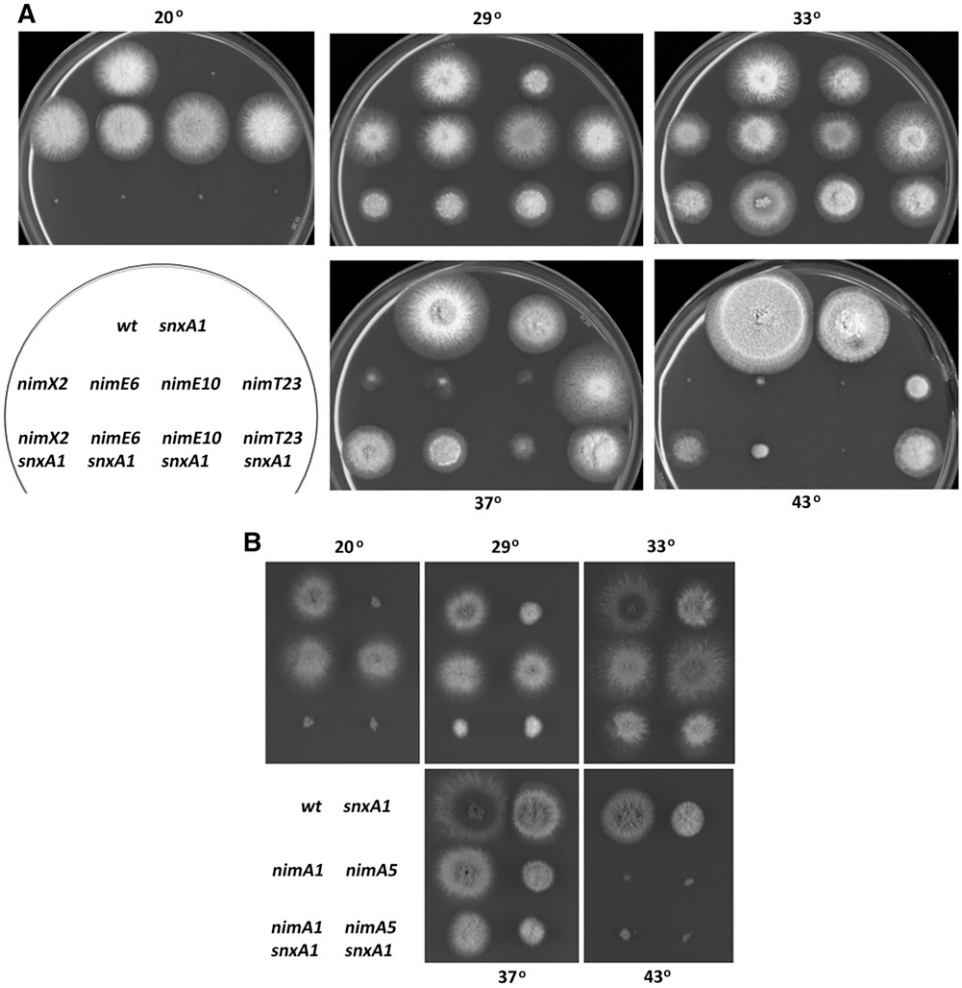

Figure 2 *snx*A1 suppresses mutations in multiple components of the CDC2/CYCLINB cell cycle regulatory pathway but not mutations in *nimA*. Growth phenotypes of single and double mutants on minimal medium at the indicated temperatures. Days of growth at each temperature are as follows: 20°, 5 days; 29°/33°/37°, 2.5 days; 43°, 3.5 days. (A) Growth phenotypes of single and double mutants in the CDC2/CYCLINB pathway. (B) Growth phenotypes of single and double mutants in *nimA*.

that (1) the *snxA1* mutation lies upstream of exon 3 or (2) overexpression of partially functional *snxA1* mutant protein was able to fully rescue *snxA1* phenotypes. We also generated *alcA*-driven cDNAs from the 9- and 11-exon alternatively spliced cDNAs described in *Materials and Methods*. The 9-exon cDNA contains 27 nt of 5′ UTR. Three different 11-exon cDNA versions were tested, containing 32, 39, or 162 nt of 5′ UTR sequence. No upstream ATGs occur in these four UTR sequences. Overexpression of each cDNA from a single copy at the *argB* locus complemented *snxA1* to varying degrees (Figure S9).

Typically, an exonic mutation can be complemented by integration of promoter-less cDNAs at the endogenous locus to restore a wild-type allele under control of the native promoter. However, in transformations with plasmid-borne *alcA*::*snxA* cDNAs, neither the 11- nor the 9-exon cDNAs were able to complement *snxA1* on glucose, *i.e.*, in an ethanol-independent manner, in 167 *argB*+ transformants with the 11-exon cDNA and in a total of 70 *argB*+ transformants obtained by using the 9-exon cDNA. There is very little difference in length and sequence of the two cDNAs (Figure S6). The two additional N-terminal exons in the 11-exon cDNA encode only nine amino acids; these two exons are interrupted by unusually long introns of 766 and 548 nt. The 9-exon cDNA begins within the 548-nt second intron (42 nt upstream of the intron 2, 3′ splice junction) and encodes 14 N-terminal amino acids by which it differs from the 11-exon cDNA (Figure S6). Given that these two cDNAs are therefore identical except at a small region in the N terminus, the absence among transformants of constitutive restoration of the wild-type phenotype suggests that (1) the *snxA1* mutation may lie within an intron or an upstream regulatory region; (2) the mutation may lie so close to the coding region N terminus as to preclude the likelihood of a crossover event between the N terminus of the cDNA and the mutation at the endogenous locus; or (3) the *snxA1* alteration may affect chromatin structure and function in the *snxA* region.

We amplified and sequenced the AN3739 genomic region in *snxA1*, spanning 5882 nucleotides from nt 3,224,102 to 3,218,220 (*Aspergillus* Genome Database: http://www.aspgd.org). The sequenced region begins 85 nt before the AN3738 start codon and 671 nt upstream of the start site of the longest 11-exon *snxA* cDNA (nt 3,213,431). This cDNA start site precedes the exon 1 start codon by 162 nt. The 5′ sequenced region contains a 100-nt-long leucyl-tRNA gene that ends 333 nt upstream of the cDNA start site. The 3′ region includes the AN3739 3′ UTR, 3′ flanking intergenic region, and the adjacent gene AN3740. The *snxA1* sequenced region extends >1000 nt beyond both ends of the 3353-nt sequence that fully complemented *snxA1* and *snxA2* in transformations

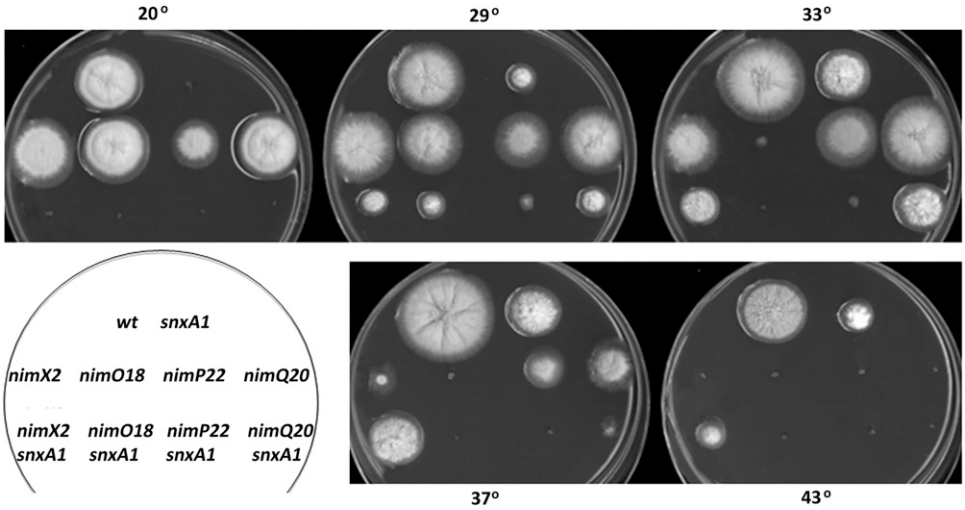

Figure 3 *snxA1* is not a general suppressor of cell cycle defects. Growth phenotypes of single and double mutants on rich medium at the indicated temperatures. Three G1- or S-phase cell cycle mutations (*nimO18*, *nimP22*, and *nimQ20*) were tested for suppression by *snxA1* and compared with the G2-M cell cycle mutation *nimX2*. Days of growth at each temperature are as follows: 20°, 7 days; 29°/33°/37°/43°, 2.5 days.

with a linear wild-type DNA fragment (Figure 6). *snxA2* was sequenced across 4842 nt from nt 3,223,063, which lies 82 nt upstream of the 3353-nt *snxA1/snxA2* linear complementing DNA region, and ends at 3,218,220, as for *snxA1* (above). Three independent PCR products each from one wild-type strain (PCS 439), a minimum of two *snxA1* strains (SWJ 3676, SWJ 3678, SWJ 3404, or SWJ 2862), and two *snxA2* strains (EAK 5496 and EAK 5497) were sequenced on both strands, for a total of at least six *snxA1* and six *snxA2* mutant-derived PCR products at each interval, and compared with the published genomic sequence derived from strain FGSC A4 (*Aspergillus* Comparative Sequencing Project, Broad Institute of Harvard and MIT; http://www.broadinstitute.org/). In addition, *snxA1* was sequenced more extensively in the 5′ flank plus exons 1 and 2 and introns 1 and 2 from nt 3,223,572 (141 nt upstream of the startsite of the 11-exon cDNA) to 3,221,861 (1711 nt), over three intervals, with at least 10 templates (20 sequences) and as many as 16 templates (33 sequences) per interval. Without exception, no DNA sequence changes were detected in *snxA1* or *snxA2*.

Multiple lines of genetic and phenotypic evidence indicate that AN3739 is *snx*A: First, classical genetic mapping localized the mutation to a small interval on chromosome II. Second, plasmid subclones containing only the wild-type AN3739 DNA complemented the *snxA1* mutation. Third, both *snxA1* and *snxA2* were efficiently complemented by a linear 3.353-kb fragment spanning most of the AN3739 locus. Finally, the fully recessive *snxA1* and *snxA2* mutations failed to complement a deletion of AN3739, indicating that these three mutations are allelic. Phenotypic support for AN3739 being *snxA* is evident in that deletion of *snxA* phenocopies *snxA1* and *snxA2* in both cold sensitivity and suppression of *nimX2*. Conversely, overexpression of wild-type and *snxA1* mutant genomic clones and alternatively spliced AN3739 cDNAs complemented *snxA1* and *ΔsnxA* when integrated as a single copy at the *argB* locus; and importantly, overexpression of a *snxA*+ gDNA abrogated the suppression of *nimX2* by *snxA1*. Therefore, despite the absence of DNA sequence changes in the *snxA1* and *snxA2* ORFs and their upstream and downstream flanking regions, we conclude that *snxA* (AN3739) encodes the single *A. nidulans* homolog of *S. cerevisiae* Hrb1/Gbp2 and human hnRNP-M.

snxA1 and snxA2 mutations decrease snxA expression

Because deletion of *snxA* phenocopies both the *snxA1* and *snxA2* mutations, we hypothesized that the hypomorphic *snxA1* and *snxA2* phenotypes are due to decreased *snxA* expression. mRNA transcript levels were quantitated in randomly cycling vegetative mycelia in *snxA1*, *snxA2*, and *snxA*$^+$ strains using qRT-PCR. Both *snxA1* and *snxA2* exhibited fivefold decreased expression relative to wild type (Figure 7A). To investigate the effects of *snxA1* and *snxA2* mutations on the levels of protein, the *snxA1*, *snxA2*, and *snxA*$^+$ alleles were tagged with a $(GA)_3$GFDGA-myc9 epitope, and their levels were detected by Western blotting from randomly cycling, vegetative mycelia grown in liquid media. As predicted, SNXA levels were greatly reduced or absent in both mutants (Figure 7B). Thus, the hypomorphic phenotypes caused by both *snxA1* and *snxA2* are due to decreased expression of *snxA*.

SNXA1 does not affect NIMX2^{CDC2} kinase activity

To determine if SNXA affects the levels of NIMX^{CDC2} protein or NIMX^{CDC2}/NIME^{CYCLINB} kinase activity, histone ^{1}H kinase assays and Western blots were performed using total protein extracts from strains carrying *snxA+/nimX+*, *snxA+/nimX2*, *snxA1/nimX+*, or *snxA1/nimX2* grown at 32° or germinated at 32° and then shifted for 3 hr to the *nimX2* restrictive temperature of 42° (Figure 8). No differences in NIMX^{CDC2} protein levels were evident in any of the strains at permissive temperature or after shifting to restrictive temperature. However, strains harboring the *nimX2* mutation had lower NIMX2^{CDC2}/NIME^{CYCLINB} kinase activity at permissive temperature. Furthermore, NIMX2^{CDC2}/NIME^{CYCLINB} kinase activity decreased in both the *snxA+/nimX2* and *snxA1/nimX2* strains after shifting to 42° (Figure 8, lanes 6 and 8). These experiments, which were repeated three times with identical results, strongly suggest that *snxA1* suppression of *nimX2* does not occur by increasing the activity of NIMX2^{CDC2}/NIME^{CYCLINB}.

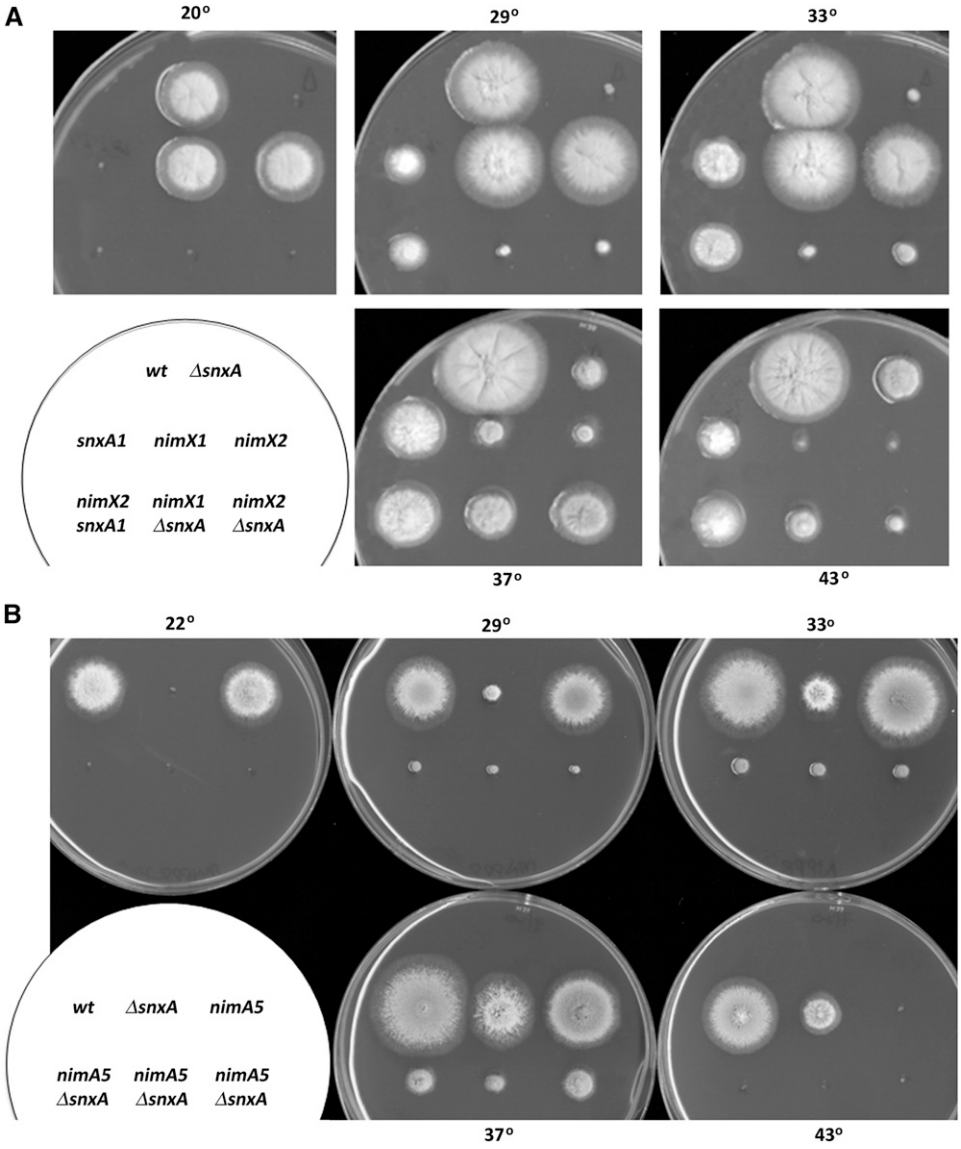

Figure 4 *ΔsnxA* suppresses *nimX*^{cdc2} mutations but does not suppress the *nimA5* G2-M defect. (A) Growth phenotypes of *nimX*$^{-}$ single and *nimX*$^{-}$ *ΔsnxA* double mutants on rich medium at the indicated temperatures. Days of growth at each temperature are as follows: 19°, 6 days; 29°/33°/37°/43°, 3 days. (B) Growth phenotypes of three independent *nimA5 ΔsnxA* double mutants at the indicated temperatures. Days of growth at each temperature are as follows: 22°, 5 days; 29°, 2.5 days; 33°/37°/43°, 2 days.

SNXA localizes to the nucleus during interphase

To localize SNXA^{HRB1} in cells, snxA was C-terminally tagged with green fluorescent protein (GFP) and monomer red fluorescent protein (mRFP) by three-way fusion PCR, followed by one-step gene replacement. A very strong nuclear signal was present in 97% of randomly cycling cells, with diffuse signal in 3% of cells, as demonstrated by colocalization with DAPI-stained nuclei (Figure 9A). SNXA::mRFP was observed in the nucleoplasm but appeared to be excluded from the nucleolus because both SNXA::mRFP and DAPI were excluded from this area. In asynchronous cultures, ~97% of nuclei were in interphase and 3% were mitotic. The high proportion of cells with nuclear SNXA::mRFP (97%) suggests that SNXA is not concentrated in the nucleus during semiclosed mitosis, during which protein localization has been hypothesized to be regulated by diffusion and localized binding (De Souza *et al.* 2004). Thus, the observed pattern suggests that SNXA^{HRB1} nuclear localization is not required at mitosis. To determine if SNXA^{HRB1} is nuclear during interphase but exits the nucleus at mitosis, strains harboring C-terminally tagged SNXA::GFP or SNXA::mRFP were combined with the following heat-sensitive mutations: *nimX2*^{cdc2}, *nimE6*^{cyclinB}, or *nimT23*^{cdc25}, which are slightly leaky G2-specific mutations; or *nimO18*^{dbf4}, a highly heat-sensitive G1/S mutation that prevents DNA replication and undergoes mitotic catastrophe, leading to mitotic arrest at restrictive temperature (James *et al.* 1999). As shown in Figure 9B, localization of SNXA^{HRB1} was predominantly nuclear in *nimX2*^{cdc2}, *nimE6*^{cyclinB}, and *nimT23*^{cdc25} cells at all temperatures. However, as *nimO18* cells began to enter mitotic arrest at the semipermissive temperature of 29° and were fully arrested at 37°, nuclear localization of SNXA^{HRB1} decreased to 0%. The entire cell was diffusely stained during mitotic arrest, suggesting that SNXA^{HRB1} exits the nucleus during mitosis.

To demonstrate that SNXA^{HRB1} exits the nucleus during mitosis, a strain with SNXA::mRFP and GFP::α-tubulin was studied. Approximately 97% of randomly cycling cells had nuclear SNXA::mRFP and an interphase array of microtubules

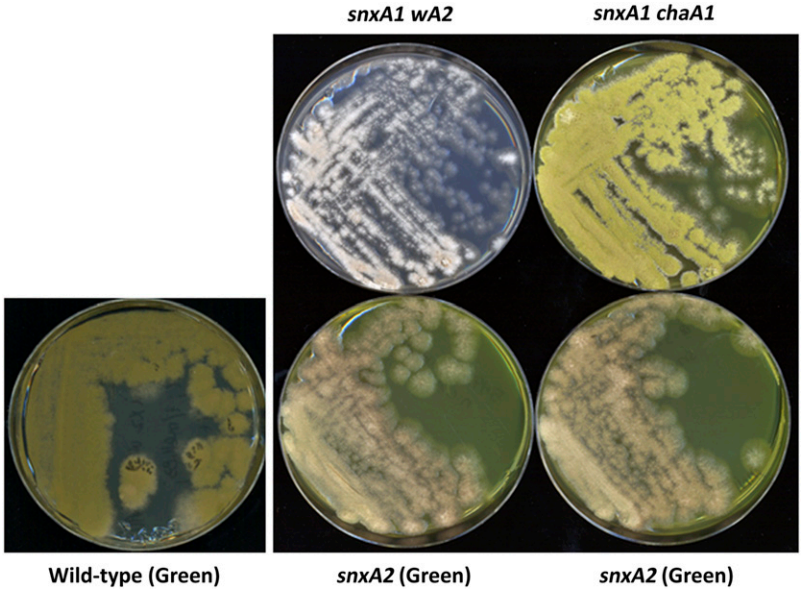

Figure 5 The *snxA2* defect is more severe than that of *snxA1*. *snxA1* strains harboring white (*wA2*) and chartreuse (*chaA1*) spore color mutations (top row), and green *snxA2* strains (bottom row) were streaked onto minimal medium and grown for 3 days at 37°. The brownish coloration of the *snxA2* strains reflects the absence of green conidia, demonstrating weaker growth at 37°.

(Figure 10). Conversely, 100% of hypha with mitotic spindles ($n > 200$) were devoid of nuclear SNXA::mRFP and exhibited a diffusely stained cytoplasm. This demonstrates that $SNXA^{HRB1}$ exits the nucleus during mitosis before formation of the mitotic spindle.

snxA1 and ΔsnxA affect NIME^{CYCLINB} localization

As discussed earlier, proper localization of mitotic kinases is essential for mitotic progression. Because *snxA1* does not suppress *nimX2* by affecting either its protein or activity levels, we suspected that it may affect the localization of $NIMX^{CDC2}$/$NIME^{CYCLINB}$. The levels of $NIME^{CYCLINB}$ could be monitored using a strain harboring GFP-labeled $NIME^{CYCLINB}$ (Nayak *et al.* 2010) (kind gift of Berl Oakley). We reasoned that because $NIMX^{CDC2}$ is active as a protein kinase only when bound to $NIME^{CYCLINB}$ (Osmani *et al.* 1994), and because its nuclear localization mirrors that of $NIME^{CYCLINB}$ (Nayak *et al.* 2010), if *snxA1* affects the localization of $NIME^{CYCLINB}$, this could also affect $NIMX^{CDC2}$/$NIME^{CYCLINB}$ localization. Wu *et al.* (1998) and Nayak *et al.* (2010) previously characterized $NIME^{CYCLINB}$ as having predominantly nuclear localization during interphase (~50–60% of hyphae had nuclear localization at interphase) and localization during mitosis that was characterized by diffuse staining of the entire hypha. To determine if either *snxA1* or Δ*snxA* affect the localization of $NIME^{CYCLINB}$, we generated strains harboring the GFP-tagged $NIME^{CYCLINB}$ together with *snxA+*, *snxA1*, Δ*snxA*, *nimX2*, or *snxA1/nimX2* by crossing strain LO1578 (kind gift of Berl Oakley) with strains having various *snxA* backgrounds. LO1578 harbors GFP-$NIME^{CYCLINB}$ under control of the endogenous *nimE* promoter; the fusion protein was reported to be fully functional and to cause no apparent mitotic or cell cycle defects (Nayak *et al.* 2010). We determined the levels of GFP-$NIME^{CYCLINB}$ in randomly cycling vegetative mycelia from *snxA+*, *snxA1*, and Δ*snxA* strains grown at 33° and found that mutation or deletion of *snxA* does not alter the expression of GFP-$NIME^{CYCLINB}$ (Figure S11). The resulting strains were germinated and the percentage of germlings (containing two to eight nuclei) with predominantly nuclear GFP-$NIME^{CYCLINB}$ were quantitated at the *snxA1* restrictive temperature (20°), *nimX2* restrictive temperature (44°), *nimX2* semipermissive temperature (37°), or permissive temperature (32°).

As shown in Figure 11, wild-type germlings (*snxA+/nimX+*) exhibited ~50–60% nuclear GFP-$NIME^{CYCLINB}$ at all temperatures tested, in agreement with published data (Wu *et al.* 1998). Because *snxA1* was originally identified as a suppressor of *nimX2*, we also studied GFP-$NIME^{CYCLINB}$ localization in *nimX2* mutants. *nimX2/snxA+* germlings exhibited nuclear GFP-$NIME^{CYCLINB}$ similar to that of wild-type germlings at 20°, but the levels increased at permissive and semipermissive temperatures and approached 85% during the slightly leaky G2 arrest (44°). This increase in nuclear GFP-$NIME^{CYCLINB}$ would be expected as the germlings arrest in G2. As in wild-type cells, GFP-$NIME^{CYCLINB}$ localization of *nimX+/snxA1* and *nimX+/ΔsnxA* germlings was consistent over a range of temperatures, but was slightly lower at all temperatures compared to wild-type germlings, ranging from 5% to 20% lower than in wild-type cells. Whereas *nimX2/snxA1* germlings generally mirrored wild type at 20°, 32°, and 37°, 50% fewer cells showed nuclear localization at 44°, relative to wild type.

Given that $NIME^{CYCLINB}$ exits the nucleus at mitosis, one possible reason for decreased nuclear localization of GFP-$NIME^{CYCLINB}$ in *snxA1/ΔsnxA* cells could be an increase in mitotic index. To determine if the localization differences were due to an increased percentage of cells in mitosis, which would lead to a drop in the percentage of cells with nuclear GFP-$NIME^{CYCLINB}$ due to its destruction at the metaphase-to-anaphase transition, the chromosome mitotic index was assessed in these same strains under the same conditions. Due to fluorescence interference, mitotic index could not be assessed in the same slides as nuclear $NIME^{CYCLINB}$; thus $NIME^{CYCLINB}$ localization and chromosome mitotic index were measured in

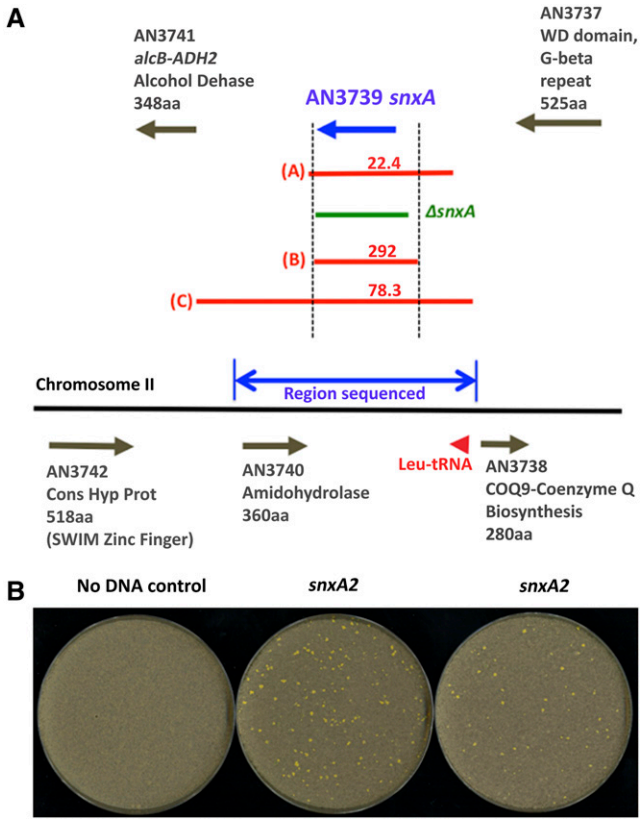

Figure 6 Complementation of *snxA1* snd *snxA2* by linear DNA fragments. *snxA1* strains tSWJ 5573/5574 and *snxA2* strains tSWJ 5567/5584, containing a deletion of *nkuA* (Ku70), were transformed with a PCR-derived linear DNA fragment of 3897 nt (panel A, red "A") and two plasmid-derived linear DNA fragments of 3530 nt (panel A, red "B") and 6686 nt (panel A, red "C"). Transformants were grown at 21° for 11 days to select for complementation of cold sensitivity. (A) Complementation results. Single arrows denote genes in the *snxA* region. Red lines indicate linear fragments used for transformation. Green line indicates the region deleted in Δ*snxA* strains. Numbers in red indicate the number of *snxA2*-complementing transformants per microgram of DNA. Blue double-arrow indicates the region sequenced in *snxA1* and *snxA2* mutants. (B) *snxA2* transformants complemented by the shortest, 3530-nt linear DNA fragment.

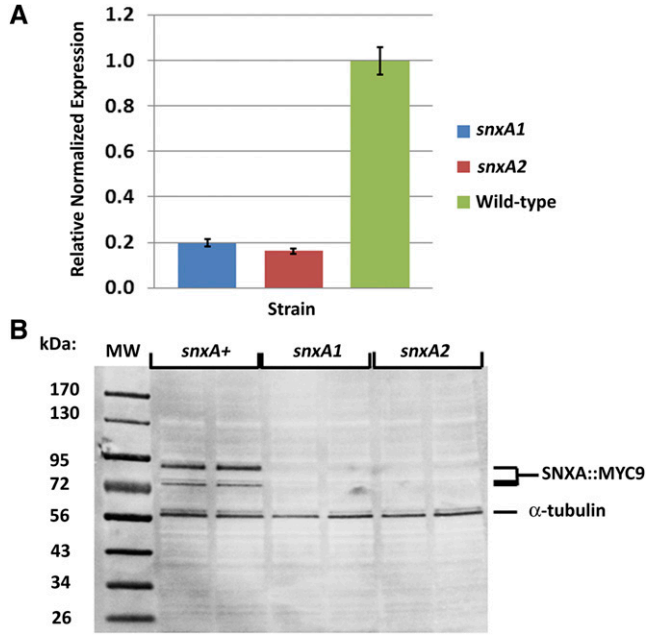

Figure 7 *snxA* mRNA and protein levels are reduced in *snxA* mutants. (A) To determine relative *snxA* mRNA expression, qRT-PCR analysis of randomly cycling vegetative mycelia was performed on *snxA*+, *snxA1*, and *snxA2* strains. Relative expression was normalized to *actA* and calculated using the ΔΔCt method. Data shown are the average relative normalized expression from six replicates. Bars = SEM. (B) To determine relative SNXA protein levels, colorimetric Western analysis of total protein extracts from randomly cycling vegetative mycelia of myc9-tagged *snxA*+, *snxA1*, and *snxA2* strains was performed. Blots were probed with mAb mycA7, washed, and reprobed with anti-α-tubulin mAb as a loading control.

separate experiments. The percentage of mitotic cells in all strains at permissive temperatures was between 2 and 4%, except at 44°, where *nimX2/snxA*+ germlings were 0.5% mitotic and *nimX2/snxA1* germlings were 6% mitotic. Although we have conservatively reported a small increase in mitotic index (to 6%) in the *snxA1/nimX2* double mutant at 44°, repeated observations in these cells (data not shown) gave variable mitotic indices as high as 10–15%. It is not possible to determine the percentage of mitotic cells below 25° in strains containing deleted or mutated *snxA* due to the accumulation of nuclear abnormalities. These data therefore demonstrate a temperature-dependent perturbation of nuclear NIME$^{\text{CYCLINB}}$ localization in *snxA*-deficient strains.

Discussion

Multiple lines of evidence reveal that in *A. nidulans* SNXA$^{\text{HRB1}}$ plays an important role in cell cycle progression, functioning both at G1 and G2. At G2, *snxA1* and *snxA2* affect the *A. nidulans* CDK1, NIMX$^{\text{CDC2}}$. In addition to isolation of the cold-sensitive, G1-arresting *snxA1* mutation as an extragenic suppressor of *nimX2* (McGuire *et al.* 2000), which arrests cells in G2 at elevated temperatures, we demonstrate here that *snxA1* suppression is not allele-specific and that *snxA1* also suppresses mutations in two heat-sensitive, G2-specific regulators of NIMX$^{\text{CDC2}}$: NIME6$^{\text{CYCLINB}}$ and NIMT23$^{\text{CDC25}}$. In contrast, *snxA1* exhibits little or no suppression of the G2-arresting *nimA1* and *nimA5* mutations, of the S-arresting *nimE10*$^{\text{cyclinB}}$ mutation, or of three G1- and S-phase-specific mutations. Functional NIMA is required for the partial disassembly of nuclear pore complexes, which allows mitotic regulators to enter the nucleus (De Souza *et al.* 2003, 2004); together with the specific suppression of CDK1 pathway mutations, the lack of suppression of *nimA* mutations by mutation or deletion of *snxA* suggests that SNXA specifically affects the CDK1 pathway. Deletion of *snxA* phenocopies the *snxA1* and *snxA2* mutations in its cold sensitivity and suppression of *nimX2*, suggesting that *snxA1* and *snxA2* are hypomorphic alleles and further supporting the finding that *snxA* interacts genetically with *nimX*. That *snxA1* and *snxA2* are hypomorphic alleles was verified by qRT-PCR and immunoblotting.

Our previous results using double reciprocal hydroxyurea block/release assays showed that at reduced temperatures *snxA1* leads to a nonreversible cell cycle arrest in G1 that

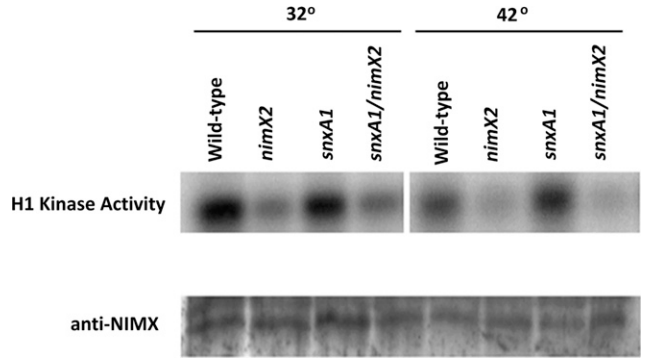

Figure 8 SNXA does not affect NIMX^{CDC2} histone ^{1}H kinase activity. To determine if *snxA1* suppresses *nimX2* by affecting NIMX protein levels or activity, *snxA+/nimX+* (lanes 1 and 5), *nimX2* (lanes 2 and 6), *snxA1* (lanes 3 and 7) and *snxA1/nimX2* (lanes 4,8) were grown at the *nimX2* permissive temperature (32°) or germinated at 32° and shifted to restrictive temperature (42°) for 2 hr. Histone ^{1}H kinase assays were performed on anti-NIMX immunoprecipitates followed by SDS-PAGE. A total of 100 ug total protein was separated by SDS-PAGE, blotted to nitrocellulose, and detected with anti-NIMX antibody E77.

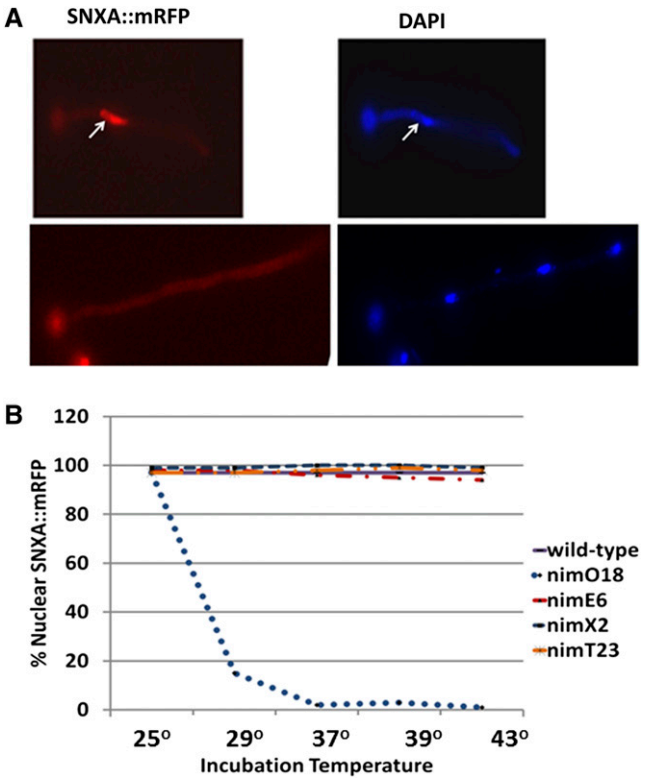

Figure 9 SNXA localizes to the nucleus in 97% of randomly cycling cells. Three-way fusion PCR was used to C-terminally tag SNXA by one-step gene replacement. Following transformation of *A. nidulans* with PCR products, gene replacement with *snxA*::mRFP::*pyrG* or *snxA*::GFP::*pyrG* was confirmed by *trans*-locus PCR and Southern blot. Fluorescence microscopy was performed to visualize SNXA::mRFP and SNXA::GFP. Strains harboring various cell cycle mutations were crossed with transformants to obtain strains with either SNXA::mRFP or SNXA::GFP and specific cell cycle mutations (*nimO18*, *nimE6*, or *nimX2*). (A) Fluorescence micrographs showing nuclear (top) and non-nuclear (bottom) localization of SNXA::mRFP at 32°. Germlings were stained with DAPI after fixation to colocalize SNXA::mRFP to nuclei. Arrows indicate nucleoli. (B) SNXA::mRFP or SNXA::GFP strains with indicated cell cycle mutations were inoculated into liquid minimal media on coverslips, incubated at the indicated temperatures for 16 hr, and visualized by fluorescence microscopy. A total of 200 germlings per strain was counted and scored for nuclear *vs.* non-nuclear SNXA::mRFP or SNXA::GFP localization.

causes gross nuclear abnormalities after prolonged incubation at 19° (McGuire *et al.* 2000). We repeated these experiments with *snxA1* strains used here, with identical results (data not shown). Given that NIMX^{CDC2} functions both at G1 and G2 (Osmani *et al.* 1994), it is not surprising that a suppressor of *nimX2* has effects at G1 and G2.

The nature of the *snxA1* and *snxA2* defects is at present mysterious. Given that both alleles failed to complement *ΔsnxA*, we conclude that they are allelic with the deletion. Moreover, a linear wild-type fragment spanning the 3′ half of intron 1 through exon 11 could efficiently complement *snxA1* and *snxA2* cold sensitivity. Both alleles were isolated after mutagenesis with the UV-mimetic, 4-NQO, leading to the expectation that they would harbor point mutations or other DNA sequence alterations. Initially, we found that (1) overexpression from a heterologous locus of an *alcA*::*snxA1* 9-exon genomic clone complemented *snxA1* as efficiently as *alcA*::*snxA*+ and (2) both 9- and 11-exon *alcA*-driven cDNAs, lacking their own promoters, could not rescue *snxA1* in an *alcA*-independent manner, *i.e.*, by crossing over to loop the plasmids into the *snxA* locus. These somewhat incongruous findings could be explained if the mutations were located in the region spanning the 3′ half of intron 1 to a region slightly downstream of intron 2. However, despite extensive sequencing within and beyond the entire *snxA* locus, and exhaustive sequencing of the region containing the promoter, 5′ UTR, exons 1–3 and introns 1–2, no DNA sequence changes were found in *snxA1* or *snxA2*.

How, then, to explain the dramatically reduced expression of apparently wild-type SNXA protein in the two mutants, which in turn suppresses defects in the CDK1 mitotic induction pathway? A DNA sequence mutation in a distant *snxA/*AN3739 regulatory element lying outside the sequenced region could lead to reduced expression and failure to complement among *snxA* alleles. However, a distant mutation should not be rescued by linear wild-type DNA fragments corresponding to the *snxA* locus, unless perhaps this mutated element (or gene) alters chromatin structure/function at the *snxA* locus. Nonetheless, to address this possibility a series of 17 overlapping linear fragments (~4 kb each) covering 38,180 nt, extending from AN3735 (nt 3,231,933) to AN4748 (nt 3,193,753), were transformed into *snxA1* and *snxA2* strains. Only AN3739-overlapping fragments complemented the mutations (Figure 6 and data not shown). Although it seems unlikely, we cannot rule out the possibility of a more distant *snxA* regulatory mutation.

More likely is the possibility that *snxA1* and *snxA2* defects may result from altered chromatin structure and function in the *snxA* region, such as by an increase in repressive histone marks or a decrease in activating marks. *A. nidulans* lacks DNA methylation (Lee *et al.* 2008) and thus a chromatin

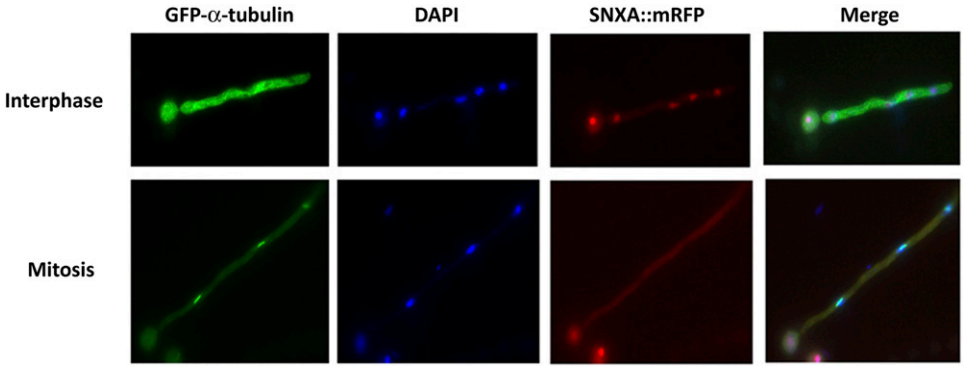

Figure 10 SNXA::mRFP is absent from the nucleus during mitosis. A strain carrying SNXA::mRFP was crossed with a strain harboring *alcA*::GFP::α-tubulin. A double-tagged strain was inoculated into minimal media onto coverslips and incubated 14 hr at 29°, followed by fixation, DAPI staining, and visualization by fluorescence microscopy. One hundred percent of hyphae with mitotic spindles ($n > 200$) were devoid of nuclear SNXA::mRFP and exhibited a diffusely stained cytoplasm.

immunoprecipitation approach, using antibodies against a variety of modified histones, may be required to reveal the biochemical nature of *snxA* defects. Of interest in this regard is the recent finding of a functional relationship between the Set1/COMPASS complex (Set1c), an H3K4 methyltransferase, and both the CDK1 and NIMA mitotic kinases, in which Set1c and the two kinases are required for mitotic induction and progression (Govindaraghavan *et al.* 2014). In general, H3K4 di- and trimethylation by Set1c has been associated with gene activation in euchromatin, and in humans has been suggested to "bookmark" active genes so that they can resume transcription following exit from mitosis (Blobel *et al.* 2009; Kelly *et al.* 2010). In *A. nidulans*, Set1c function has also been shown to mediate repression of certain secondary metabolite gene clusters that occur in subtelomeric regions (reviewed in Gacek and Strauss 2012). Given its newly discovered and poorly understood role in promoting mitosis, and the apparent role of *snxA* in restraining nuclear division, it will be of interest to determine what kind of functional relationship may exist between Set1c and *snxA*.

A recent study of *Rumplestiltskin* (*Rump*), the *Drosophila melanogaster* homolog of *snxA* and hnRNP-M, provides evidence for direct involvement in an epigenetic mechanism affecting higher-order chromatin structure through modulation of insulator function (King *et al.* 2014). *Rump* associates physically with *Drosophila* core insulator proteins, colocalizing to a subset of insulator binding sites. Depletion of *Rump* improved the enhancer-blocking and barrier function of a *gypsy* transposable element, suggesting that *Rump* acts normally to inhibit insulator activity, possibly by competing with insulator–insulator interactions. In addition to this newly discovered role in chromatin dynamics, *Rump* also autoregulates its own expression (King *et al.* 2014). These findings suggest a possible mechanisn for *snxA* in regulating the expression of G2-M regulators in *A. nidulans*. We show here that levels of $NIMX^{CDC2}$ and $NIME^{CYCLINB}$ are not affected in *snxA* mutants. However, depletion of SNXA might, for example, improve insulator function to enhance the expression of a positive regulator such as $NIMT^{CDC25}$ or to increase the repression of a negative regulator of G2-M, such as SUC1 or $ANKA^{WEE1}$.

The role of $SNXA^{HRB1}$ in cell cycle progression is further demonstrated by the observed alterations in $NIME^{CYCLINB}$ distributions in populations of *snxA1* and Δ*snxA* germlings. The depletion of $SNXA^{HRB1}$ in these cells diminishes the percentage of cells with nuclear $NIME^{CYCLINB}$. The lowest levels of nuclear $NIME^{CYCLINB}$ occurred in *nimX2/snxA1* germlings at 37° and 44°, the temperatures at which *snxA1* suppresses the *nimX2* G2 arrest to permit passage through G2/M. The decreased nuclear $NIME^{CYCLINB}$ localization in the *nimX2/snxA1* double mutant likely reflects completion of M phase. The consistent and reproducibly lower nuclear $NIME^{CYCLINB}$ localization at 37° and 44° that is less than wild-type levels suggests that these cells progress through mitosis, at which time $NIME^{CYCLINB}$ is degraded and thus no longer visible in the nucleus, and that they may be delayed in G1, giving a further reduction in nuclear $NIME^{CYCLINB}$. In other words, the observed decreased nuclear $NIME^{CYCLINB}$ at 37° and 44° in *snxA1/nimX2* mutants might seem counterintuitive, since *snxA* depletion rescues the G2 arrest of $nimX2^{CDC2}$. This rescue could occur by increased movement of $NIMX^{CDC2}$ and $NIME^{CYCLINB}$ into the nucleus. However, this rescue, by permitting mitotic progression, leads to the destruction of $NIME^{CYCLINB}$ at the metaphase-to-anaphase transition and thus can explain why $NIME^{CYCLINB}$ levels are lowest in this *snxA1/nimX2* strain at 37° and 44°.

Mitotic regulation via the CDC2/CYCLINB pathway has been shown to ultimately depend on control of CDC2/CYCLINB activity, which is tightly regulated by phosphorylation/dephosphorylation (Ye *et al.* 1995), and on proper nuclear localization of the fully active CDC2/CYCLINB complex (Wu *et al.* 1998). The finding that *snxA1* does not increase $NIMX2^{CDC2}$ protein levels or $NIMX2^{CDC2}/NIME^{CYCLINB}$ activity at the *nimX2* restrictive temperature, where *snxA1* does suppress the *nimX2* G2 arrest, suggests that the effects of SNXA1 on the $NIMX2^{CDC2}/NIME^{CYCLINB}$ mitotic initiation pathway occur by a different mechanism, such as proper localization of the active complex. Given that $NIMX^{CDC2}$ is active as a protein kinase only when bound to its regulatory subunit, $NIME^{CYCLINB}$, our findings that $NIME^{CYCLINB}$ has altered localization patterns in both *snxA1* and Δ*snxA* hyphae support this hypothesis. This is particularly interesting, given that *snxA* is homologous with *S. cerevisiae* Hrb1/Gbp2, which encode mRNA shuttling binding proteins similar to the mammalian SR family of proteins. While these proteins have been shown in budding yeast to shuttle mRNAs to the cytoplasm and to remain with the transcript during translation (Windgassen

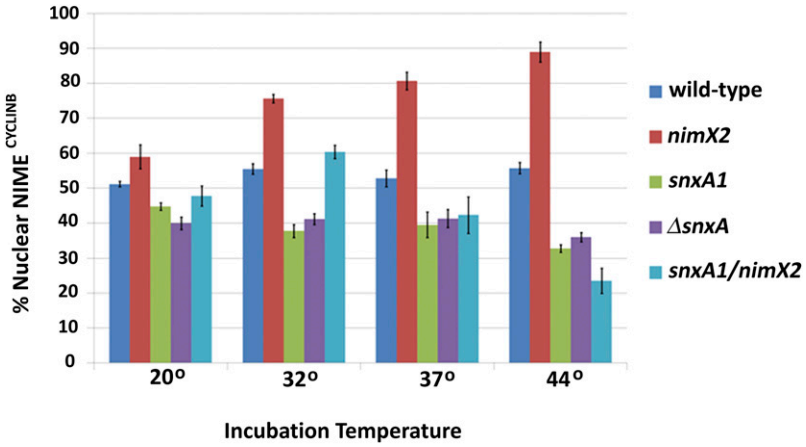

Figure 11 *snxA1* and *ΔsnxA* strains have decreased nuclear NIME^{CYCLINB}. Strains harboring the GFP-tagged NIME^{CYCLINB} together with *snxA*$^{+}$, *snxA1*, *ΔsnxA*, *nimX2*, or *snxA1/nimX2* were grown to germling stage (two to eight nuclei) at the indicated temperatures, and the number of germlings with predominantly nuclear GFP-NIME^{CYCLINB} was quantitated. The means of four to six replicates per strain are shown, with 100 germlings scored per replicate. Bars = SEM.

et al. 2004), heretofore no specific cell cycle functions have been suggested for Hrb1/Gbp2, although overexpression of Gbp2 does lead to a delay in G1 (Stevenson *et al.* 2001). Because deletion of these genes in *S. cerevisiae* does not disrupt or alter the nucleocytoplasmic distribution of bulk polyadenylated mRNAs (Hacker and Krebber 2004), it is possible that either they function as adaptors for specific subsets of mRNPs, as suggested by Rougemaille *et al.* (2008), or they may confer additional, previously unidentified functions.

With its partially closed mitosis, *A. nidulans* represents an evolutionary intermediate between the closed mitosis of budding yeast and the open mitosis of more complex eukaryotes (for review, see De Souza and Osmani 2009). It is therefore not surprising that some evolutionarily conserved proteins involved in cell cycle regulation have additional and/or different functions in different organisms. Given that the G2/M effects of SNXA^{HRB1} do not occur by modulating NIMX^{CDC2}/NIME^{CYCLINB} activity, but that *snxA* mutation or deletion alters NIME^{CYCLINB} localization patterns, it is possible that in *A. nidulans* SNXA^{HRB1} regulates the localization either of NIMX^{CDC2}/NIME^{CYCLINB} or of mitosis-specific proteins that function upstream or downstream of the activation of NIMX^{CDC2}/NIME^{CYCLINB}.

Using time-lapse imaging of cyclin B-GFP, Nayak *et al.* (2010) demonstrated that cyclin B becomes visible in the nucleoplasm and at SPBs ~40% of the way through interphase, during S phase, and confirmed observations by De Souza *et al.* (2009) that the majority of this cyclin B exits the nucleus when the NPC partially disassembles, leaving a subpool of cyclin B concentrated at SPBs and on the spindle. This subpool disappears gradually as mitosis progresses. Although it is beyond our abilities to detect, it is possible that mutation of SNXA^{HRB1} allows this subpool to remain in the nucleus longer; if so, this could allow threshold levels of NIMX2^{CDK1} protein to accumulate in *nimX2* mutants, resulting in suppression of the heat-sensitive phenotype. Alternatively, it is possible that nuclear transport is altered in *snxA* mutants, leading to the accumulation or retention of threshold levels of CDK1/CYCLINB. An additional possibility is that SNXA^{HRB1} affects proteins involved in mitotic exit; a defect in inactivation of the anaphase-promoting complex/cyclosome, as Nayak *et al.* (2010) reported in *mipAD159* mutants (γ-tubulin), could both allow threshold levels of NIMX2^{CDC2} activity to be reached and delay G1, resulting in lower nuclear NIME^{CYCLINB}. We are currently investigating these alternatives.

The dramatic decrease in SNXA^{HRB1} nuclear localization during the highly heat-sensitive pseudomitotic arrest of the *nimO18* mutation underscores the nature of the partially closed mitosis of *A. nidulans*. At mitosis, the nuclear pore complexes partially disassemble, and proteins not specifically retained in the nucleus diffuse out of the partially closed nuclear pores and may equilibrate across the nuclear envelope (De Souza *et al.* 2004); those proteins destined to return to the nucleus are likely specifically re-imported once the nuclear pores completely reassemble. SNXA^{HRB1} appears to be one of these proteins.

The identification of *snxA* as the *A. nidulans* homolog of Hrb1/Gbp2, the G1 arrest phenotype of *snxA1* mutants, the exit of SNXA^{HRB1} from the nucleus during mitosis and its subsequent re-import after mitotic exit, the NIMX^{CDC2}/NIME^{CYCLINB} activity-independent effects of *snxA* on the NIMX^{CDC2}/NIME^{CYCLINB} G2/M pathway, and the altered localization of NIME^{CYCLINB} suggest a novel function for the SNXA^{HRB1} SR family protein in eukaryotes: a function in cell cycle regulation. Moreover, the fact that reducing or eliminating *snxA* function alleviates heat-sensitive defects in *nimX*^{cdc2} mutants and in mutant regulators of *nimX*^{cdc2} activity (*nimE6*^{cyclinB} and *nimT23*^{cdc25}) suggests that *snxA* may normally act to restrain mitotic induction by the CDC2/CYCLINB regulatory pathway.

Acknowledgments

We thank Jennifer Powell (Gettysburg College), Peter Mirabito (University of Kentucky), and André Walther (Cedar Crest College) for helpful advice and suggestions; the Fungal Genetics Stock Center (Kansas City, MO) for providing genetic mapping strains, libraries, cosmids, and fosmids used in this study; Stephen Osmani (Ohio State University) for providing antibodies and strains; Xin Xiang (Uniformed Services University of the Health Sciences) for providing the GFP-α-tubulin strain; Berl Oakley (University of Kansas) for providing the

GFP-NIME^{CYCLINB} strain; Sabrice Guerrier (Millsaps College) for providing antibodies; Roy Duhe and Chetan Patil (University of Mississippi Medical Center) for assistance with kinase assays; Cory Toyota (Millsaps College) for assistance with qRT-PCR analysis; and the reviewers for helpful comments that improved this manuscript. This work was supported by grants from Gettysburg College to S.W.J.; by grants to S.L.A. from Millsaps College; by National Institutes of Health grant R15GM055885 and Mississippi *IDeA Networks of Biomedical Research Excellence* grant P20RR016476 funded by the National Institute of General Medical Sciences, National Institutes of Health to SLA; and by grants from the Howard Hughes Medical Institute to Gettysburg College and Millsaps College.

Literature Cited

Alam, M. K., A. M. El-Ganiny, S. Afroz, D. A. Sanders, J. Liu *et al.*, 2012 Aspergillus nidulans galactofuranose biosynthesis affects antifungal drug sensitivity. Fungal Genet. Biol. 49: 1033–1043.

Bachewich, C., K. Masker, and S. Osmani, 2005 The polo-like kinase PLKA is required for initiation and progression through mitosis in the filamentous fungus Aspergillus nidulans. Mol. Microbiol. 55: 572–587.

Ballance, D. J., F. P. Buxton, and G. Turner, 1983 Transformation of Aspergillus nidulans by the orotidine-5′-phosphate decarboxylase gene of Neurospora crassa. Biochem. Biophys. Res. Commun. 112: 284–289.

Blobel, G. A., S. Kadauke, E. Wang, A. W. Lau, J. Zuber *et al.*, 2009 A reconfigured pattern of MLL occupancy within mitotic chromatin promotes rapid transcriptional reactivation following mitotic exit. Mol. Cell 36: 970–983.

Brody, H., J. Griffith, A. J. Cuticchia, J. Arnold, and W. E. Timberlake, 1991 Chromosome-specific recombinant DNA libraries from the fungus Aspergillus nidulans. Nucleic Acids Res. 19: 3105–3109.

De Souza, C. P., and S. A. Osmani, 2009 Double duty for nuclear proteins: the price of more open forms of mitosis. Trends Genet. 25: 545–554.

De Souza, C. P., K. P. Horn, K. Masker, and S. A. Osmani, 2003 The SONB(NUP98) nucleoporin interacts with the NIMA kinase in *Aspergillus nidulans*. Genetics 165: 1071–1081.

De Souza, C. P., A. H. Osmani, S. B. Hashmi, and S. A. Osmani, 2004 Partial nuclear pore complex disassembly during closed mitosis in Aspergillus nidulans. Curr. Biol. 14: 1973–1984.

De Souza, C. P., S. B. Hashmi, T. Nayak, B. Oakley, and S. A. Osmani, 2009 Mlp1 acts as a mitotic scaffold to spatially regulate spindle assembly checkpoint proteins in Aspergillus nidulans. Mol. Biol. Cell 20: 2146–2159.

Gacek, A., and J. Strauss, 2012 The chromatin code of fungal secondary metabolite gene clusters. Appl. Microbiol. Biotechnol. 95: 1389–1404.

Galagan, J. E., S. E. Calvo, C. Cuomo, L. J. Ma, J. R. Wortman *et al.*, 2005 Sequencing of Aspergillus nidulans and comparative analysis with A. fumigatus and A. oryzae. Nature 438: 1105–1115.

Govindaraghavan, M., S. L. Anglin, A. H. Osmani, and S. A. Osmani, 2014 The Set1/COMPASS histone H3 methyltransferase helps regulate mitosis with the CDK1 and NIMA mitotic kinases in *Aspergillus nidulans*. Genetics 197: 1225–1236.

Hacker, S., and H. Krebber, 2004 Differential export requirements for shuttling serine/arginine-type mRNA-binding proteins. J. Biol. Chem. 279: 5049–5052.

Hackmann, A., H. Wu, U. M. Schneider, K. Meyer, K. Jung *et al.*, 2014 Quality control of spliced mRNAs requires the shuttling SR proteins Gbp2 and Hrb1. Nat. Commun. 5: 3123.

Harris, S. D., J. L. Morrell, and J. E. Hamer, 1994 Identification and characterization of *Aspergillus nidulans* mutants defective in cytokinesis. Genetics 136: 517–532.

Hung, C. J., Y. J. Lee, D. H. Chen, and C. Li, 2009 Proteomic analysis of methylarginine-containing proteins in HeLa cells by two-dimensional gel electrophoresis and immunoblotting with a methylarginine-specific antibody. Protein J. 28: 139–147.

Hurt, E., M. J. Luo, S. Rother, R. Reed, and K. Strasser, 2004 Cotranscriptional recruitment of the serine-arginine-rich (SR)-like proteins Gbp2 and Hrb1 to nascent mRNA via the TREX complex. Proc. Natl. Acad. Sci. USA 101: 1858–1862.

James, S. W., P. M. Mirabito, P. C. Scacheri, and N. R. Morris, 1995 The Aspergillus nidulans bimE (blocked-in-mitosis) gene encodes multiple cell cycle functions involved in mitotic checkpoint control and mitosis. J. Cell Sci. 108(Pt 11): 3485–3499.

James, S. W., K. A. Bullock, S. E. Gygax, B. A. Kraynack, R. A. Matura *et al.*, 1999 nimO, an Aspergillus gene related to budding yeast Dbf4, is required for DNA synthesis and mitotic checkpoint control. J. Cell Sci. 112(Pt 9): 1313–1324.

Kafer, E., 1977 Meiotic and mitotic recombination in Aspergillus and its chromosomal aberrations. Adv. Genet. 19: 33–131.

Kaminskyj, S. G. W., 2001 Fundamentals of growth, storage, genetics and microscopy of *Aspergillus nidulans*. Fungal Genet. Newsl. 48: 25–31.

Kelly, T. K., T. B. Miranda, G. Liang, B. P. Berman, J. C. Lin *et al.*, 2010 H2A.Z maintenance during mitosis reveals nucleosome shifting on mitotically silenced genes. Mol. Cell 39: 901–911.

Kim Guisbert, K., K. Duncan, H. Li, and C. Guthrie, 2005 Functional specificity of shuttling hnRNPs revealed by genome-wide analysis of their RNA binding profiles. RNA 11: 383–393.

King, M. R., L. H. Matzat, R. K. Dale, S. J. Lim, and E. P. Lei, 2014 The RNA-binding protein Rumpelstiltskin antagonizes gypsy chromatin insulator function in a tissue-specific manner. J. Cell Sci. 127: 2956–2966.

Lee, D. W., M. Freitag, E. U. Selker, and R. Aramayo, 2008 A cytosine methyltransferase homologue is essential for sexual development in Aspergillus nidulans. PLoS ONE 3: e2531.

Lindqvist, A., V. Rodriguez-Bravo, and R. H. Medema, 2009 The decision to enter mitosis: feedback and redundancy in the mitotic entry network. J. Cell Biol. 185: 193–202.

Liu, H. L., A. H. Osmani, L. Ukil, S. Son, S. Markossian *et al.*, 2010 Single-step affinity purification for fungal proteomics. Eukaryot. Cell 9: 831–833.

Livak, K. J., and T. D. Schmittgen, 2001 Analysis of relative gene expression data using real-time quantitative PCR and the 2 (-Delta Delta C(T)). Method. Methods 25: 402–408.

Lleres, D., M. Denegri, M. Biggiogera, P. Ajuh, and A. I. Lamond, 2010 Direct interaction between hnRNP-M and CDC5L/PLRG1 proteins affects alternative splice site choice. EMBO Rep. 11: 445–451.

Ma, H. T., and R. Y. Poon, 2011 How protein kinases co-ordinate mitosis in animal cells. Biochem. J. 435: 17–31.

McGuire, S. L., D. L. Roe, B. W. Carter, R. L. Carter, S. P. Grace *et al.*, 2000 Extragenic suppressors of the *nimX2*(cdc2) mutation of *Aspergillus nidulans* affect nuclear division, septation and conidiation. Genetics 156: 1573–1584.

Nakajima, K., and Y. Yaoita, 1997 Construction of multiple-epitope tag sequence by PCR for sensitive Western blot analysis. Nucleic Acids Res. 25: 2231–2232.

Nayak, T., E. Szewczyk, C. E. Oakley, A. Osmani, L. Ukil *et al.*, 2006 A versatile and efficient gene-targeting system for *Aspergillus nidulans*. Genetics 172: 1557–1566.

Nayak, T., H. Edgerton-Morgan, T. Horio, Y. Xiong, C. P. De Souza *et al.*, 2010 Gamma-tubulin regulates the anaphase-promoting

complex/cyclosome during interphase. J. Cell Biol. 190: 317–330.

Nielsen, J. B., M. L. Nielsen, and U. H. Mortensen, 2008 Transient disruption of non-homologous end-joining facilitates targeted genome manipulations in the filamentous fungus Aspergillus nidulans. Fungal Genet. Biol. 45: 165–170.

Nigg, E. A., 1995 Cyclin-dependent protein kinases: key regulators of the eukaryotic cell cycle. BioEssays 17: 471–480.

O'Connell, M. J., A. H. Osmani, N. R. Morris, and S. A. Osmani, 1992 An extra copy of nimEcyclinB elevates pre-MPF levels and partially suppresses mutation of nimTcdc25 in Aspergillus nidulans. EMBO J. 11: 2139–2149.

Osherov, N., and G. May, 2000 Conidial germination in *Aspergillus nidulans* requires RAS signaling and protein synthesis. Genetics 155: 647–656.

Osmani, S. A., D. B. Engle, J. H. Doonan, and N. R. Morris, 1988 Spindle formation and chromatin condensation in cells blocked at interphase by mutation of a negative cell cycle control gene. Cell 52: 241–251.

Osmani, A. H., S. L. McGuire, and S. A. Osmani, 1991 Parallel activation of the NIMA and p34cdc2 cell cycle-regulated protein kinases is required to initiate mitosis in A. nidulans. Cell 67: 283–291.

Osmani, A. H., N. van Peij, M. Mischke, M. J. O'Connell, and S. A. Osmani, 1994 A single p34cdc2 protein kinase (encoded by nimXcdc2) is required at G1 and G2 in Aspergillus nidulans. J. Cell Sci. 107(Pt 6): 1519–1528.

Osmani, A. H., J. Davies, H. L. Liu, A. Nile, and S. A. Osmani, 2006 Systematic deletion and mitotic localization of the nuclear pore complex proteins of Aspergillus nidulans. Mol. Biol. Cell 17: 4946–4961.

Ovechkina, Y., P. Maddox, C. E. Oakley, X. Xiang, S. A. Osmani *et al.*, 2003 Spindle formation in Aspergillus is coupled to tubulin movement into the nucleus. Mol. Biol. Cell 14: 2192–2200.

Pontecorvo, G., J. A. Roper, L. M. Hemmons, K. D. Macdonald, and A. W. Bufton, 1953 The genetics of Aspergillus nidulans. Adv. Genet. 5: 141–238.

Porat, Z., O. Erez, and C. Kahana, 2006 Cellular localization and phosphorylation of Hrb1p is independent of Sky1p. Biochim. Biophys. Acta 1763: 207–213.

Reed, R., and H. Cheng, 2005 TREX, SR proteins and export of mRNA. Curr. Opin. Cell Biol. 17: 269–273.

Rougemaille, M., T. Villa, R. K. Gudipati, and D. Libri, 2008 mRNA journey to the cytoplasm: attire required. Biol. Cell 100: 327–342.

Sanford, J. R., N. K. Gray, K. Beckmann, and J. F. Caceres, 2004 A novel role for shuttling SR proteins in mRNA translation. Genes Dev. 18: 755–768.

Stevenson, L. F., B. K. Kennedy, and E. Harlow, 2001 A large-scale overexpression screen in Saccharomyces cerevisiae identifies previously uncharacterized cell cycle genes. Proc. Natl. Acad. Sci. USA 98: 3946–3951.

Strasser, K., and E. Hurt, 2000 Yra1p, a conserved nuclear RNA-binding protein, interacts directly with Mex67p and is required for mRNA export. EMBO J. 19: 410–420.

Thandapani, P., T. R. O'Connor, T. L. Bailey, and S. Richard, 2013 Defining the RGG/RG motif. Mol. Cell 50: 613–623.

Todd, R. B., M. A. Davis, and M. J. Hynes, 2007 Genetic manipulation of Aspergillus nidulans: heterokaryons and diploids for dominance, complementation and haploidization analyses. Nat. Protoc. 2: 822–830.

Tuck, A. C., and D. Tollervey, 2013 A transcriptome-wide atlas of RNP composition reveals diverse classes of mRNAs and lncRNAs. Cell 154: 996–1009.

Waring, R. B., G. S. May, and N. R. Morris, 1989 Characterization of an inducible expression system in Aspergillus nidulans using alcA and tubulin-coding genes. Gene 79: 119–130.

Warkocki, Z., P. Odenwalder, J. Schmitzova, F. Platzmann, H. Stark *et al.*, 2009 Reconstitution of both steps of Saccharomyces cerevisiae splicing with purified spliceosomal components. Nat. Struct. Mol. Biol. 16: 1237–1243.

Windgassen, M., D. Sturm, I. J. Cajigas, C. I. Gonzalez, M. Seedorf *et al.*, 2004 Yeast shuttling SR proteins Npl3p, Gbp2p, and Hrb1p are part of the translating mRNPs, and Npl3p can function as a translational repressor. Mol. Cell. Biol. 24: 10479–10491.

Wu, L., S. A. Osmani, and P. M. Mirabito, 1998 A role for NIMA in the nuclear localization of cyclin B in Aspergillus nidulans. J. Cell Biol. 141: 1575–1587.

Xu, G., X. D. Gao, J. H. Lee, H. Huang, H. Tan *et al.*, 2014 Cell type-restricted activity of hn RNPM promotes breast cancer metastasis via regulating alternative splicing. Genes Dev. 28: 1191–1203.

Yang, L., L. Ukil, A. Osmani, F. Nahm, J. Davies *et al.*, 2004 Rapid production of gene replacement constructs and generation of a green fluorescent protein-tagged centromeric marker in Aspergillus nidulans. Eukaryot. Cell 3: 1359–1362.

Ye, X. S., G. Xu, R. T. Pu, R. R. Fincher, S. L. McGuire *et al.*, 1995 The NIMA protein kinase is hyperphosphorylated and activated downstream of p34cdc2/cyclin B: coordination of two mitosis promoting kinases. EMBO J. 14: 986–994.

Yu, J. H., Z. Hamari, K. H. Han, J. A. Seo, Y. Reyes-Dominguez *et al.*, 2004 Double-joint PCR: a PCR-based molecular tool for gene manipulations in filamentous fungi. Fungal Genet. Biol. 41: 973–981.

Communicating editor: D. Lew

GENETICS

Supporting Information
http://www.genetics.org/lookup/suppl/doi:10.1534/genetics.114.167445/-/DC1

Restraint of the G2/M Transition by the SR/RRM Family mRNA Shuttling Binding Protein SNXA^{HRB1} in *Aspergillus nidulans*

Steven W. James, Travis Banta, James Barra, Lorela Ciraku, Clifford Coile, Zach Cuda, Ryan Day, Cheshil Dixit, Steven Eastlack, Anh Giang, James Goode, Alexis Guice, Yulon Huff, Sara Humbert, Christina Kelliher, Julie Kobie, Emily Kohlbrenner, Faustin Mwambutsa, Amanda Orzechowski, Kristin Shingler, Casey Spell, and Sarah Lea Anglin

DOI: 10.1534/genetics.114.167445

A. **B.**

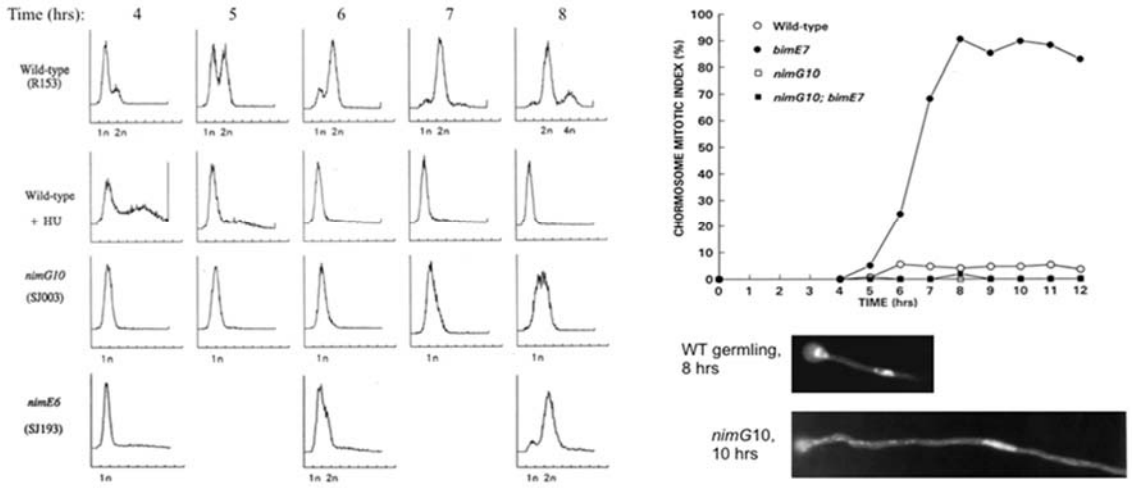

Figure S1 *nimE*10^{CYCLINB} arrests in S phase. (A) Flow cytometric analysis of DNA content of *nimE*10^{cyclinB} (formerly *nimG*10) and *nimE*6^{cyclinB} cells. Conidia were germinated at 44°. For comparison with mutants, wild-type cells were germinated in the absence or presence of the DNA synthesis inhibitor hydroxyurea (HU, 50 mM). Samples were withdrawn hourly (WT and SWJ 003) or every other hour (SWJ 193) beginning at 4 hours, fixed in ethanol, and stained with propidium iodide as described in James *et al*. (1995). Linear fluorescence histograms show relative DNA content in arbitrary units on the horizontal axis, and the cell number on the vertical axis. Each histogram is based on counts of 10,000 cells. (B) Chromosome mitotic index and nuclear morphology of the *nimE*10^{cyclinB} mutant at restrictive temperature. Conidia were germinated at 44° for 12 hours in Kafer's minimal medium. Beginning at 4 hours, samples were taken hourly and fixed and stained with DAPI to determine nuclear number and chromosome mitotic index, as described in James *et al*. (1995). For each sample, at least 150 individual cells were scored at 100x magnification on a Zeiss Axioplan or Nikon Optiphot photomicroscope equipped with epifluorescence optics. ○, Wild type (R153); ●, *bimE*7 (SWJ 010); □, *nimE*10 (SWJ 1614); ■, *nimE*10 *bimE*7 (SWJ 144). Photomicrographs depict a representative wild-type cell harboring two interphase nuclei, each with a single nucleolus, after 8 hours of germination at 44°; and a representative *nimE*10 cell arrested at the restrictive temperature with a single interphase nucleus lacking a nucleolus (x1350 magnification), after germination for 10 hours. Note the elongated hypha and multiple mitochondrial DNAs, indicated by the small bright dots distributed through the cell.

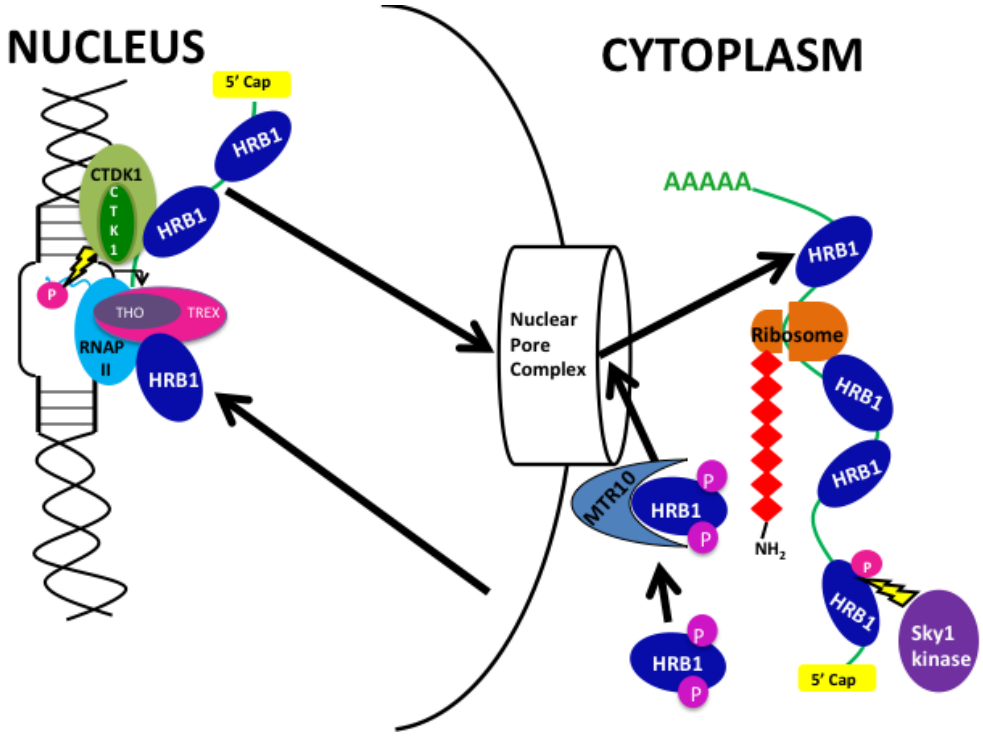

Figure S2 Functions of Hrb1 in *Saccharomyces cerevisiae.* Hrb1p, a serine-arginine rich protein with conserved RNA binding domains, is a shuttling mRNA binding protein that associates with newly transcribed RNA as part of the messenger ribonucleoprotein complex (mRNP). Hrb1p associates with the TREX complex and with Ctk1, facilitating phosphorylation of the C-terminal domain of RNA polymerase II by CTDKI, and thereby promoting elongation. The mRNP is exported from the nucleus via the nuclear pore complex (NPC), and subsequently delivered to the translational machinery. Hrb1p directs the mature mRNA to ribosomes, and remains associated with the transcript throughout translation. Hrb1p is also phosphorylated by Sky1p in the cytoplasm, increasing Hrb1p affinity for mRNA. The Mtr10 karyopherin import receptor returns Hrb1p to the NPC (Reed & Cheng, 2005; Porat et al., 2006).

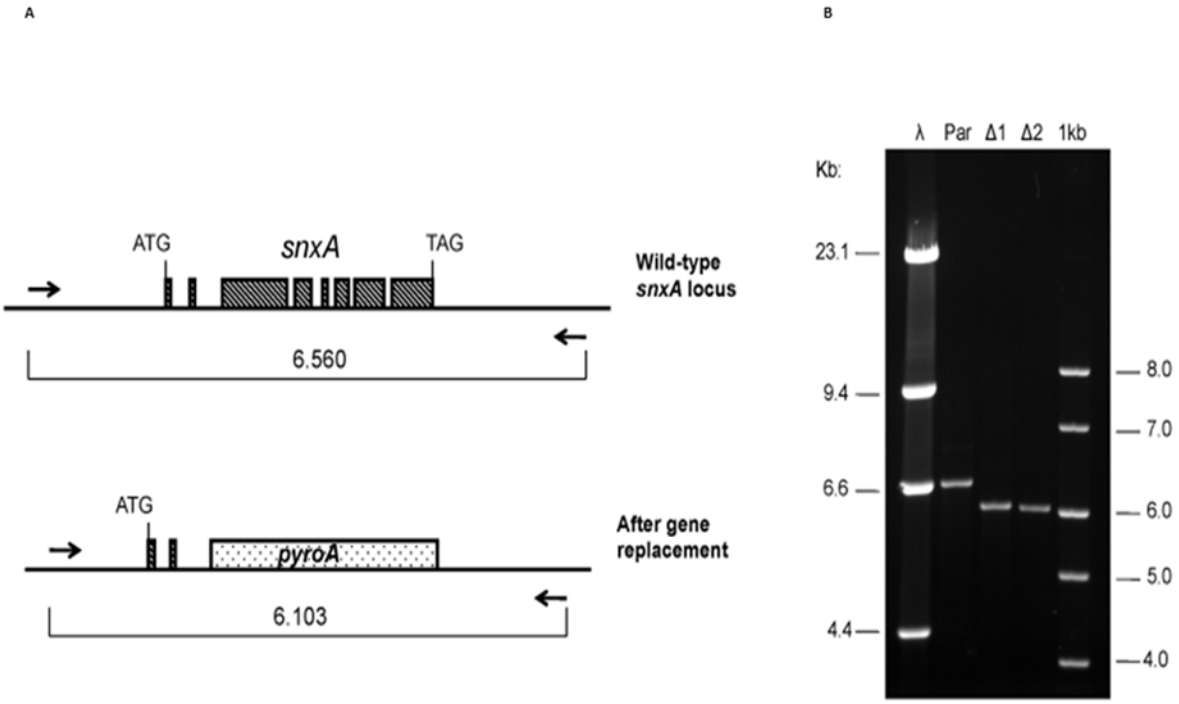

Figure S3 *snxA* deletion. *snxA+* (AN3739) was deleted from tSWJ 2973 (*pyrG*89; *pyroA*4 Kutr-L::*pyrG*^{Af}; *nicA*2; *riboB*2) by one-step replacement with *A. fumigatus pyroA*. **A**. Gene deletion strategy. Arrows indicate the position of PCR primers that lie outside of the linear DNA used to delete *snxA*. The primers should amplify a 6.56 kb product from the parent *snxA*+ strain, and a 6.1 kb product from the deleted locus. **B.** Trans-locus PCR of the parent *snxA*+ strain and two *ΔsnxA::pyroA* transformants. Key to lanes: λ, Lambda *Hind*III DNA size markers; Par, tSWJ 2973 *snxA*+ parent; Δ1 & Δ2 , tSWJ 4412/4413 Δ*snxA::pyroA* transformants; 1kb, 1kb ladder.

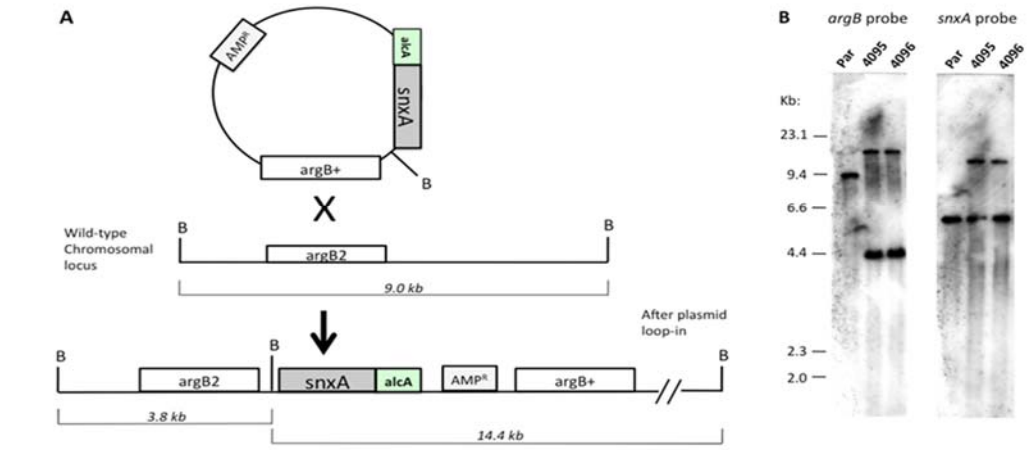

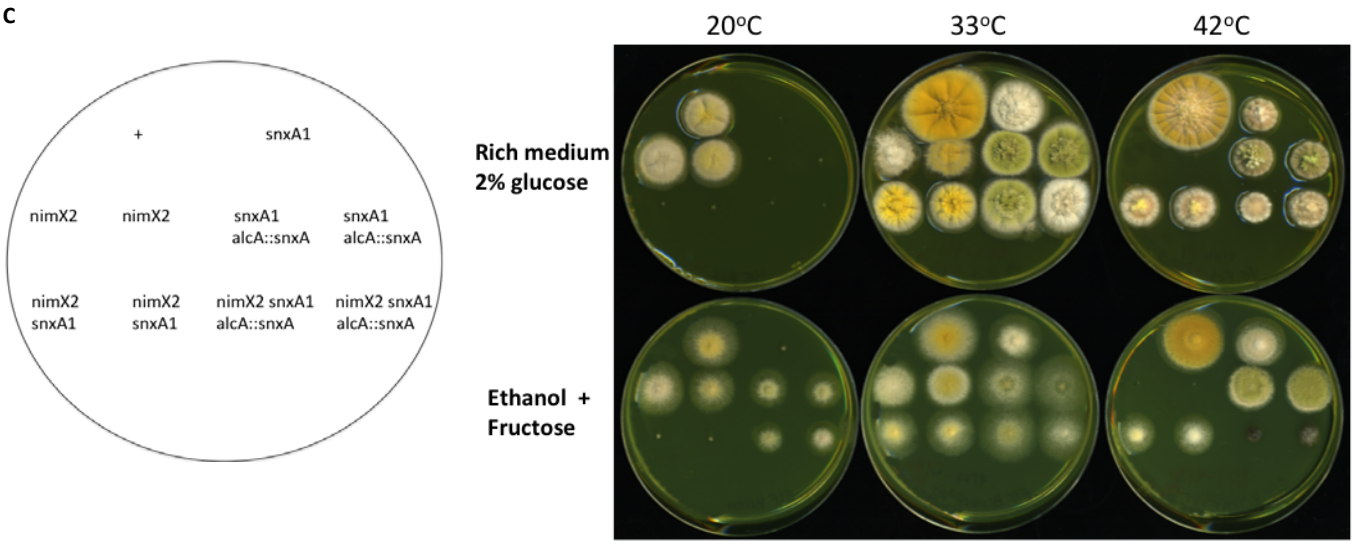

Figure S4 *alcA::snxA* construct. A *snxA*$^{+}$ wild-type 9-exon genomic clone was fused with the *alcA* alcohol dehydrogenase gene promoter as described in Materials & Methods. An *alcA::snxA*-containing plasmid was transformed into a *snxA*1 strain (SWJ 3676: *ribo*A1; *snx*A1; *argB*2; *pyroA*4; *cha*A1), and *argB*$^{+}$ transformants were recovered and purified. Total genomic DNAs were digested with *BamH*I and subjected to Southern blotting. (A) Southern blot strategy for plasmid integration at the *argB* locus. B, *BamH*I. (B) Southern blots were analyzed using probes corresponding to the coding regions of *Aspergillus nidulans argB* and *snxA*. When probed with *argB*, single-copy integration at the *argB* locus should replace the 9.0 kb wild-type *BamH*I band with two bands of 3.8 and 14.4 kb, respectively. Probing the same blot with *snxA* should produce a 6 kb band corresponding to the wild-type *snxA* locus, and a 14.4 kb band corresponding to integration at *argB*. Par, parental strain; 4095 & 4096, tSWJ 4095 and tSWJ 4096 (cf. Table S1). (C) *snxA*$^{+}$ overexpression rescues pleiotropic *snx*A1 phenotypes. An *alcA*-driven copy of wild-type

snxA (*alcA::snxA*$^{+}$) was integrated at the *argB* locus, and then combined in strains bearing *snxA*1 or *snxA*1 + *nimX*2 mutations. Complementation of *snxA*1 cold-sensitive and suppressor phenotypes was assessed by comparing growth at three temperatures during *alcA* repression (rich media containing 2% glucose) or *alcA* induction (minimal media containing 200mM ethanol + 0.04% fructose). Strains were point-inoculated using conidia from fresh streaks. Two representative strains of each genotype are shown. Plates were incubated for the following times: 20°C, 10 days; 33°C and 42°C, 3 days.

$(GA)_3$GFDGA-myc9 DNA sequence:

ATCGATGGAGCTGGAGCAGGTGCGGGATTCGATGGAGCTGAACAGAAACTTATTTCTGAAGAAGATCTTGGTGCTGAACAGAAACT
TATTTCTGAAGAAGATCTTGGTGCTGAACAGAAACTTATTTCTGAAGAAGATCTTGGTGCTGAACAGAAACTTATTTCTGAAGAAG
ATCTTGGTGCTGAACAGAAACTTATTTCTGAAGAAGATCTTGGTGCTGAACAGAAACTTATTTCTGAAGAAGATCTTGGTGCTGAA
CAGAAACTTATTTCTGAAGAAGATCTTGGTGCTGAACAGAAACTTATTTCTGAAGAAGATCTTGGTGCTGAACAGAAACTTATTTC
TGAAGAAGACCTTGGTGCTATCAAGTGAAAGCTT

$(GA)_3$GFDGA -myc9 peptide sequence:

GAGAGAGFDGAEQKLISEEDLGAEQKLISEEDLGAEQKLISEEDLGAEQKLISEEDLGAEQKLISEEDLGAEQKLISEEDLGAEQK
LISEEDLGAEQKLISEEDLGAEQKLISEEDLGAIK*

MW of this 121 aa peptide = 12,912

Blue nucleotide sequence indicates optimal forward PCR primer

Red indicates vector sequences (*BspD*I and *Hind*III)

myc tag sequence = 10aa E Q K L I S E E D L

Primer pairs for cassette amplification and gene tagging:

$(GA)_3$GFDGA -myc9-5R: (use this reverse complement as marker tail for the 5' flank fusion primer):

5' CGC ACC TGC TCC AGC TCC 3'

Pair this primer with each of the following selectable marker tails:

3' *pyroA*:
5' GGT TCA TTC TTG TTA GGG TGT TCT GTG C 3'

3' *pyrG*:
5' CAT CAC GCA TCA GTG CCT CCT CTC AGA C 3'

3' *riboB*:
5' CGT CAC ACT CAT GTA ACG GTT CTG C 3'

```
Sequence: 17-9-T7 GA5-myc9 9-22-11 Range: 1 to 378

                10        20        30        40        50
           ATCGATGGAGCTGGAGCAGGTGCGGGATTCGATGGAGCTGAACAGAAACT
           TAGCTACCTCGACCTCGTCCACGCCCTAAGCTACCTCGACTTGTCTTTGA
            I   D   G   A   G   A   G   A   G   F   D   G   A   E   Q   K   L


                60        70        80        90       100
           TATTTCTGAAGAAGATCTTGGTGCTGAACAGAAACTTATTTCTGAAGAAG
           ATAAAGACTTCTTCTAGAACCACGACTTGTCTTTGAATAAAGACTTCTTC
             I   S   E   E   D   L   G   A   E   Q   K   L   I   S   E   E
```

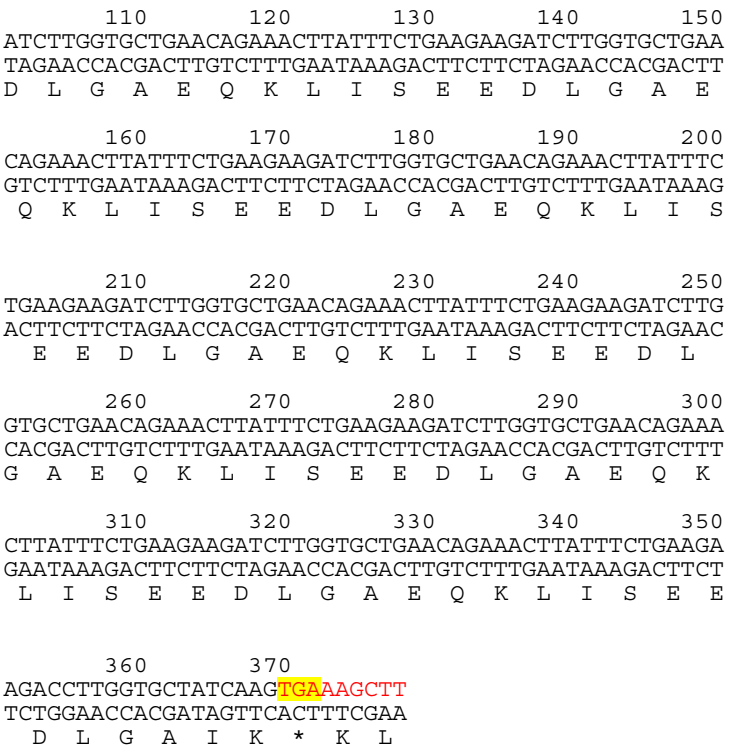

Figure S5 $(GA)_3$GFDGA -myc9 universal tagging cassettes

A. CLUSTAL W (1.83) multiple sequence alignment

```
snxA_11_exon_479aa   MADVYRPY-----QRERSRSPRRRSRSPRR-------------------
snxA_9_exon_484aa    MPYGDYEYDTDRAQRERSRSPRRRSRSPRR-------------------
YNL004W_HRB1Sc       MSDQERGSENNNRSRSRSRSPVRRRMSDDHGYERDNHLSRRSGNYNGRRK
YCL011C_GBP2Sc       M-ERELGMYGN--DRSRSRSPVRRRLSDDRDRY-DDYNDSSSNNGNGSR-
                     *            .*.***** **  *  :

snxA_11_exon_479aa   ----------------------SRRSYSPRSRSRSRDRDDYRR-----
snxA_9_exon_484aa    ----------------------SRRSYSPRSRSRSRDRDDYRR-----
YNL004W_HRB1Sc       FADTYRGSRDRGEYRGGRERSDYRERERFNNRDNPRSRDRYDDRRRGRDV
YCL011C_GBP2Sc       -----RQRRDRG----------------------SRFNDRYDQSYG----
                                                     .* .** *

snxA_11_exon_479aa   ----SDRRSRSPMS---AAQGPSGGHS---GSGYSGRGGSYPPP-PRSFE
snxA_9_exon_484aa    ----SDRRSRSPMS---AAQGPSGGHS---GSGYSGRGGSYPPP-PRSFE
YNL004W_HRB1Sc       TGRYGNRRDDYPRSFRSRHNTRDD--SRRGGFGSSGARGDYGPLLARELD
YCL011C_GBP2Sc       GSRYHDDRNWPPRR---GGRGRGGSRSFRGGRG-GGRGRTLGPIVERDLE
                          : *.  *       .  ..  *   * * .*      *   *.::

snxA_11_exon_479aa   DRAVAKEQMMQSVRESSQQDRRVYVGNLSYDVKWHHLKDFMRQAGDVIFA
snxA_9_exon_484aa    DRAVAKEQMMQSVRESSQQDRRVYVGNLSYDVKWHHLKDFMRQAGDVIFA
YNL004W_HRB1Sc       STYEE--------KVNRNYSNSIFVGNLTYDSTPEDLTEFFSQIGKVVRA
YCL011C_GBP2Sc       RQFD---------ATKRNFENSIFVRNLTFDCTPEDLKELFGTVGEVVEA
                                  . : .. ::* **::* . ..*.:::   *.*: *

snxA_11_exon_479aa   DVLLLPNGMSKGCGIVEYATREQAQNAVNTLSNQNLMNRLVYVREDREPE
snxA_9_exon_484aa    DVLLLPNGMSKGCGIVEYATREQAQNAVNTLSNQNLMNRLVYVREDREPE
YNL004W_HRB1Sc       DII-TSRGHHRGMGTVEFTNSDDVDRAIRQYDGAFFMDRKIFVRQDNPPP
YCL011C_GBP2Sc       DII-TSKGHHRGMGTVEFTKNESVQDAISKFDGALFMDRKLMVRQDNPPP
                     *::  ..*  :* * **::. :..: *:   ..  :*:* : **:*. *

snxA_11_exon_479aa   P---RFSGGPSRGDFGGPGRGGFGGYGGGPGGGGRQLYVSNLPFNVGWQD
snxA_9_exon_484aa    P---RFSGGPSRGDFGGPGRGGFGGYGGGPGGGGRQLYVSNLPFNVGWQD
YNL004W_HRB1Sc       SNNIKERKALDRGELRHN-------------RKTHEVIVKNLPASVNWQA
YCL011C_GBP2Sc       EAAKEFSKKATREEIDN----------------GFEVFIINLPYSMNWQS
                         .      * ::                    :: : *** .:.**

snxA_11_exon_479aa   LKDLFRQAAQQGTVIRADVHTDASGRPKGSGIVAFESPDDARNAIQQFNG
snxA_9_exon_484aa    LKDLFRQAAQQGTVIRADVHTDASGRPKGSGIVAFESPDDARNAIQQFNG
YNL004W_HRB1Sc       LKDIFKEC---GNVAHADVELDGDGVSTGSGTVSFYDIKDLHRAIEKYNG
YCL011C_GBP2Sc       LKDMFKEC---GHVLRADVELDFNGFSRGFGSVIYPTEDEMIRAIDTFNG
                     ***:*::.   * * :***. * .* . * * * :   .:  .**: :**

snxA_11_exon_479aa   YDWQGRTLEVREDRFAGSGPGMGRGGYGGFGGRGGFGGRGGFGGRGGFGG
snxA_9_exon_484aa    YDWQGRTLEVREDRFAGSGPGMGRGGYGGFGGRGGFGGRGGFGGRGGFGG
YNL004W_HRB1Sc       YSIEGNVLDVKSKESVHN------------------------------
YCL011C_GBP2Sc       MEVEGRVLEVREGRFNKRKNNDRY-------------------------
                      . :*..*:*:. .

snxA_11_exon_479aa   GFGGRGGFGGGYGGPPSGPGFDAGPSV--PPNPFTDYATSGGEKSNTIYV
snxA_9_exon_484aa    GFGGRGGFGGGYGGPPSGPGFDAGPSV--PPNPFTDYATSGGEKSNTIYV
YNL004W_HRB1Sc       ---------HSDGDDVDIPMDDSPV--NEEARKFTENVVGGGERNRLIYC
YCL011C_GBP2Sc       -NQRREDLEDTRGTEPGL-AQDAAVHIDETAAKFTEGVNPGGDRNCFIYC
                                 *   .    *:       .  **: .  **::.  **



snxA_11_exon_479aa   RNLPWSTCNDDLVDLFSTIGKVERAEIQYEPNGRSRGTGVVQFDNADTAE
snxA_9_exon_484aa    RNLPWSTCNDDLVDLFSTIGKVERAEIQYEPNGRSRGTGVVQFDNADTAE
YNL004W_HRB1Sc       SNLPFSTAKSDLYDLFETIGKVNNAELRYDSKGAPTGIAVVEYDNVDDAD
YCL011C_GBP2Sc       SNLPFSTARSDLFDLFGPIGKINNAELKPQENGQPTGVAVVEYENLVDAD
                      ***:**...** *** .***::.**:: : :* . * .**:::*   *:

snxA_11_exon_479aa   TSIAKFTGYQYGGRPLGITFVKYLTPAQGPADPMDDAQPTGGLTQDQIM
snxA_9_exon_484aa    TSIAKFTGYQYGGRPLGITFVKYLTPAQGPADPMDDAQPTGGLTQDQIM
YNL004W_HRB1Sc       VCIERLNNYNYGGCDLDISYAKR------------------------L
YCL011C_GBP2Sc       FCIQKLNNYNYGGCSLQISYARR------------------------D
                      .* ::..*:***  * *::.:
```

B. Alignment of AN3739 (*snxAI*) with human hnRNP-M

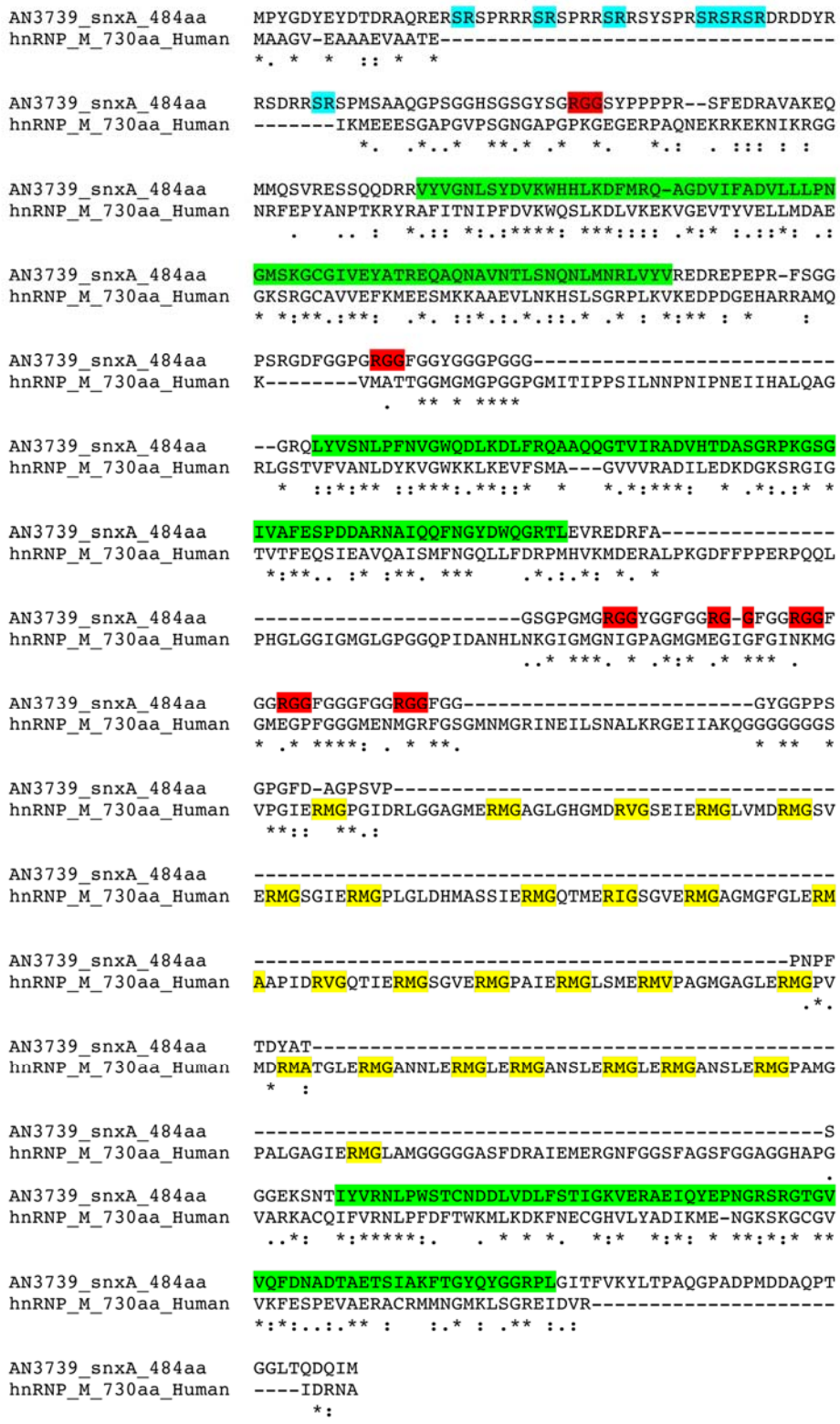

Figure S6 Alignment of SNXA cDNAs with *S. cerevisiae* and human homologs. Sequences were aligned using TCOFFEE (http://www.ebi.ac.uk/Tools/msa/tcoffee/). A. Alignment of two alternative SNXA cDNAs with *S. cerevisiae* HRB1/GBP2.

Magenta denotes alternative N-terminal peptides in SNXA cDNAs. Green, RNA Recognition Motifs (RRM); aqua in SNXA and yellow in HRB1/GBP2 denote N-terminal SR dipeptides; gray and red indicate RGG tripeptides in HRB1/GRB2 and SNXA, respectively. B. Alignment of a SNXA cDNA with human hnRNP-M. Colors as in A., except that yellow in hnRNP-M denotes RMG/RVG/RIG/RMA/RMV tripeptides.

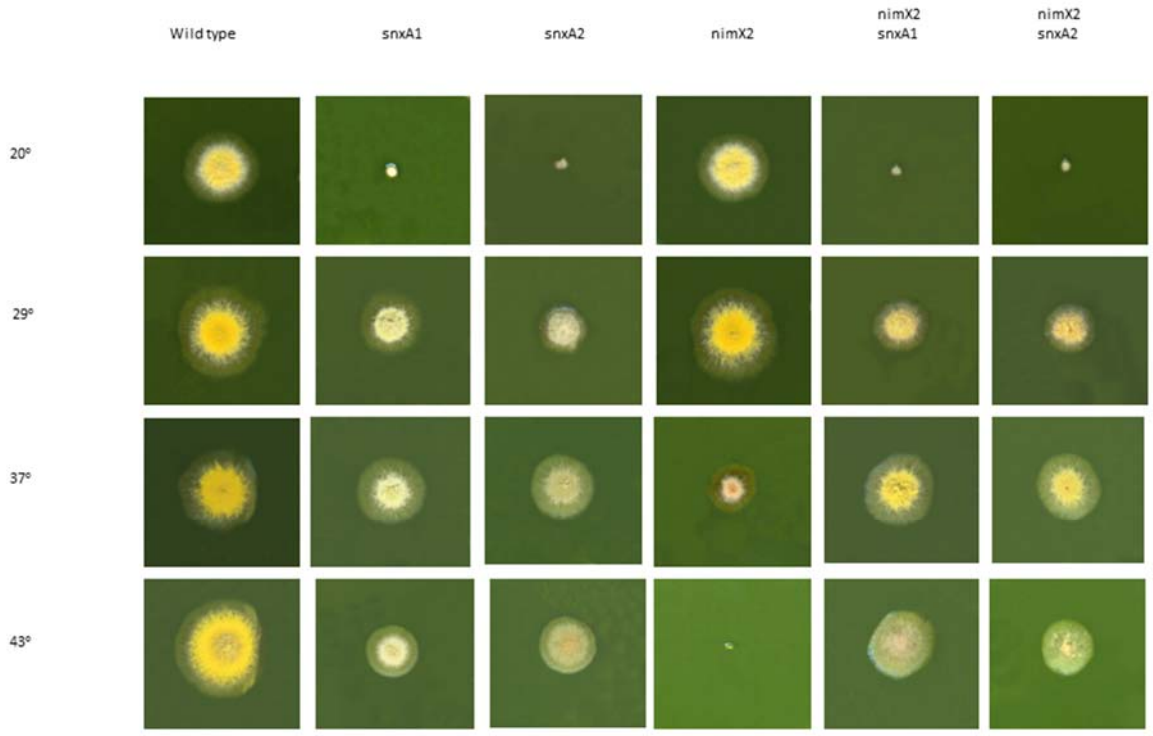

Figure S7 *snxA*2 suppresses the heat-sensitivity of *nimX*2^{cdk1}. Growth phenotypes of *snxA*1 and *snxA*2 single and *nimX*2 double mutants on minimal medium at the indicated temperatures. Days of growth at each temperature as follows: 20°, 6 days; 29°/37°/43°, 3 days.

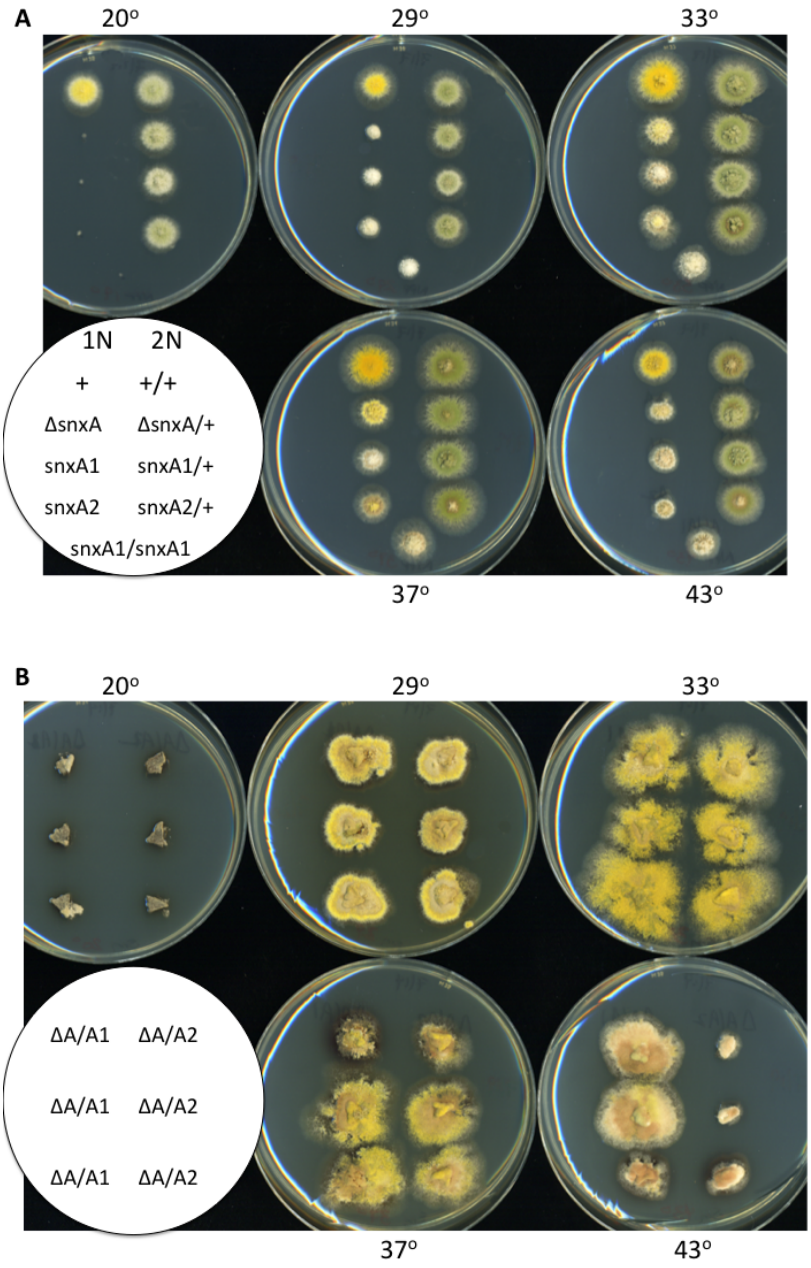

Figure S8 *snxA1* and *snxA2* are allelic with a *snxA* deletion. A. *snxA* mutations are fully recessive. Heterozygous diploids containing *ΔsnxA*, *snxA1*, or *snxA2* were synthesized, streaked three times to clonal purity, and tested for dominance or recessiveness by toothpicking conidia onto minimal medium and growing at a range of temperatures. Strains used are as follows: Haploid (1N) controls: Wild-type (+), SWJ 4050; *ΔsnxA*, tSWJ 4394; *snxA1*, SWJ 2862; *snxA2*, SWJ 5581. Diploids (2N): Wild-type (+/+), dSWJ 3799; *ΔsnxA/+*, dSWJ 5972; *snxA1/+*, dSWJ 3653; *snxA2/+*, dSWJ 5975; *snxA1/snxA1*, dSWJ 3923. Days of growth: 20°, 7 days; 29°, 2.5 days; 33°, 37°, and 43°, 2 days. B. *snxA1* and *snxA2* fail to complement a *snxA* null allele in heterokaryons. Balanced heterokaryons containing *ΔsnxA/snxA1*, or *ΔsnxA/snxA2* were established, then agar chunks from the perimeter of three independently derived heterokaryons were transferred to minimal media and grown at a range of temperatures. Strains used: *ΔsnxA/snxA1,* tSWJ 4394 x SWJ 4030; *ΔsnxA/snxA2*, tSWJ 4394 x SWJ 5562. Days of growth: 20°, 8 days; 29°, 6 days; 33°, 37°, and 43°, 5 days.

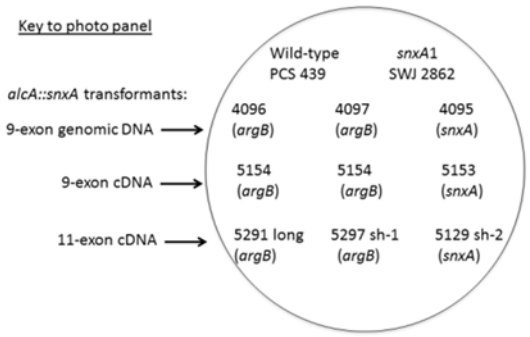

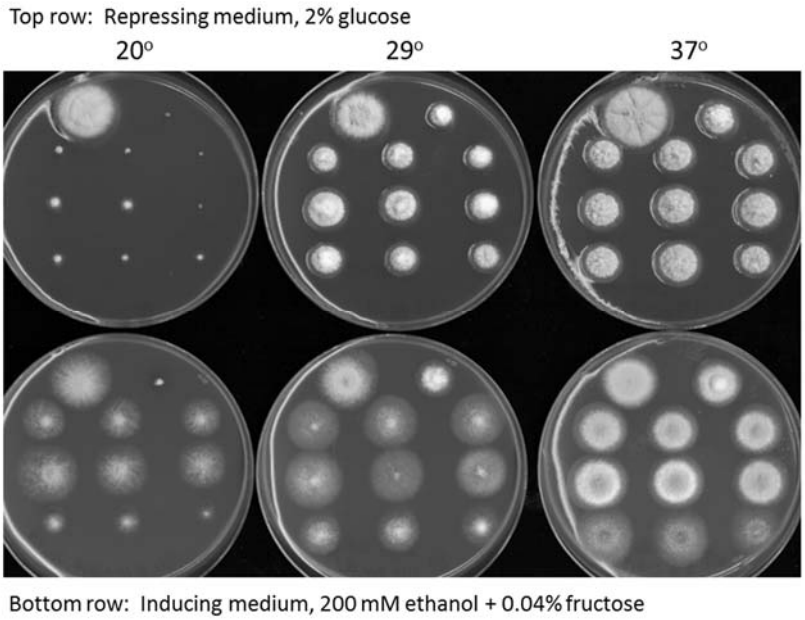

DNA sequences of 5' UTR leaders in alcA::snxA cDNA fusions in pSDW 194:

9-exon genomic DNA (4095/4096/4097) -
(*Kpn*I-*Sma*I/*Spe*I) M P Y G D
p*alcA* – GGTACCC/AGT GTC TTA **ATG** CCT TAC GGC GAC

9-exon cDNA (5153/5154) –
(*Kpn*I) M P Y G D
p*alcA* – GGTA CCT GAC CTT TAT TGT TTC GCC GTC TTA **ATG** CCT TAC GGC GAC

11-exon cDNA, short-1 UTR, *snxA* integration (5129) –
(*Kpn*I) M A D V Y
p*alcA* – GGTACC TCT GTT TGG ACA CCT CCG ACC GCG TCT TCA AC **ATG** GCC GAC GTC TAT

11-exon cDNA, short-2 UTR, *argB* integration (5297) –
(*Kpn*I) M A D
p*alcA* – GGTAC CAG CCT CTC TGT TTG GAC ACC TCC GAC CGC GTC TTC AAC **ATG** GCC GAC

11-exon cDNA, long UTR, *argB* integration (5291) –
(*Kpn*I) M A D
p*alcA* – GGTAC CTT TGT TGT GAG TTG CGG GAG GAT / *129 nt* / GTC TTC AAC **ATG** GCC GAC

KEY: 5' UTR sequences underlined; START codon in bold; single-letter amino acid sequence shown above DNA sequence

Figure S9 *snxA* cDNA overexpression complements *snxA*1 cold-sensitivity. Growth phenotypes of transformants of SWJ 3676 (*riboA*1; *snxA*1; *argB*2; *pyroA*4; *chaA*1) carrying a single copy of an *alcA::snxA* genomic or cDNA clone integrated at either the *argB* or the *snxA* locus. Integration at *argB* or *snxA* is indicated in parentheses under the strain number. Shown for the 11-exon cDNA are representative strains containing varying lengths of 5'UTR sequence between the *alcA* promoter and the cDNA start codon: long, 162 nt; sh-1 (short-1), 32 nt; sh-2, 39 nt (cf. Table S1). For *argB* integrants of the 9-exon gDNA and 11-exon cDNA, two representative transformants are shown. Strains were point-inoculated using conidia from fresh streaks. Plates were incubated for the following times in repressing medium (2% glucose): 20° - 7 days; 29° and 37° - 48 hours. Inducing medium (200 mM ethanol + 0.04% fructose): 20° – 8 days; 29° and 37° – 60 hours.

Figure S10 snxA overexpression complements a *snxA* gene deletion. Seven independently Isolated strains (tSWJ 4324/4325/4326/5187/5188/5189/5190) carrying one copy of *alcA::snxA* integrated at the *argB* locus and a deletion of the 9-exon *snxA* genomic locus were grown on *alcA* repressing medium (2% glucose) or Inducing medium (200 mM ethanol + 0.04% fructose) at the restrictive and permissive temperatures for Δ*snxA*. Days of growth: 19°, 8 days; 37°, 3 days.

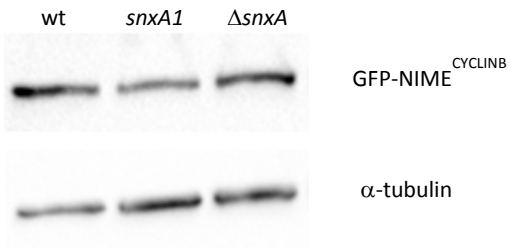

Figure S11 GFP-NIME^{CYCLINB} expression is not altered in *snxA1* or Δ*snxA* strains. Total protein extracts from strains harboring GFP-NIME^{CYCLINB} together with *snxA+* (wt), *snxA1*, or Δ*snxA* were run on SDS-PAGE, blotted to nitrocellulose, and the blot probed with anti-GFP antibody/HRP secondary antibody. The blot was stripped and re-probed with anti α-tubulin antibody/HRP secondary antibody. Strains used were the same strains as in Figure 11.

Table S1 ***Aspergillus nidulans*** **strains**

Strain	Genotype	Source
R153	*pyroA4; wA2*	SAO
SWJ 598	*pabaA1; wA2; argB2*	SWJ
SWJ 2860	*riboA1; wA3 (drkA1?)*	This study
SWJ 4050	*yA2; pyroA4; drkA1*	This study
SWJ 4357	*pabaA1 biA1; riboB2 chaA1*	This study
SWJ 4499	*pyroA4; riboB2 (pyrG89*? *Kutr-L::pyrG*?)	SWJ
SWJ 4500	*yA2; pyroA4; drkA1; riboB2 (pyrG89? Kutr-L::pyrG*?)	SWJ
BC7	*wA2 snxA1; nicB8; riboB2*	SLA
SWJ 2862	*pabaA1; wA2 snxA1 (drkA1*?)	This study
SWJ 2863	*pabaA1 riboA1; snxA1 (drkA1*?)	This study
SWJ 3406	*riboA1; snxA1; pyroA4; choA1; chaA1*	This study
SWJ 4030	*riboA1; snxA1; methB3; chaA1*	This study
A382	*yA2; adH23 AcrA1 wA3 anB8*	FGSC
A715	*proA1 yA2; hisG113; chaA1*	FGSC
A338	*yA2; wA3 puA1 cnxE16 adC1 acrB2*	FGSC
SWJ 3487	*riboA1 yA2; puA1 cnxE16 snxA1 (acrB2*?)	This study
SWJ 3545	*yA2; puA1 cnxE16 hisG113; chaA1*	This study
SWJ 3676	*riboA1; snxA1; argB2; pyroA4; chaA1*	This study
tSWJ 2353	*pyrG89; pyroA4 ΔnkuA::argB; nimO18; riboB2*	SWJ
tSWK 2888	*pabaA1; argB2; pyroA4 ⊿nkuA::argB; riboB2*	SWJ
tSWJ 2973	*pyrG89; pyroA4 Kutr-L::pyrG Af; nicA2; riboB2*	SWJ
tSWJ 4412	*pyrG89; ΔsnxA::pyroA; pyroA4; Kutr-L::pyrG; nicA2; riboB2*	This study
tSWJ 4394	*yA2; ΔsnxA::pyroA; pyroA4; nicA2*	This study
SO64	*riboA1; wA2 nimX2*^{F223L}; *nicB8*	SAO
SWJ 1597:	*wA2 nimX1*^{G225S}; *pyroA4; methB3 (yA2*? *lacA1*?)	SWJ
SWJ 1602	*yA2; wA2 nimX2*^{F223L}; *methB3 (lacA1*?)	SWJ

SWJ 1604	*yA2; nimX2*^{F223L}; *pyroA4 methB3 (lacA1*?)	SWJ
SWJ 4034	*pabaA1; wA2 nimX1*^{G225S}; *pyroA4; nicA2*	SWJ
SWJ 4501	*yA2; nimX2*^{F223L}; *pyroA4; drkA1; riboB2*	SWJ
	(*pyrG89*? *Kutr-L::pyrG?*)	
SWJ 4037	*pabaA1; wA2 nimX3*^{Y306H}; *pyroA4*	SWJ
SWJ 195	*pabaA1; nimE6 wA2 (yA2*?)	SWJ
SWJ 1614	*nimE10; methB3; chaA1 (lacA1*?)	SWJ
SWJ 170	*pabaA1; nimT23*	SWJ
SWJ 220	*pabaA1; nimT23 wA2; methB3*	SWJ
SWJ 1617	*pabaA1; nimA5; chaA1 (lacA1?)*	This study
SWJ 4202	*pabaA1; wA2 nimX1*^{G225S} *snxA1; pyroA4; riboB2*	This study
MDS 250	*riboA1; wA2 nimX2*^{F223L} *snxA1; nicB8*	SLA
SWJ 3710	*yA2; nimX2*^{F223L} *snxA1; pyroA4; methB3*	This study
SWJ 4199	*pabaA1; wA2 nimX3*^{Y306H} *snxA1*	This study
SWJ 3922	*riboA1; nimE6 snxA1*	This study
SWJ 3895	*pabaA1; nimE10 snxA1; choA1; chaA1*	This study
SWJ 4029	*wA2 nimT23 snxA1; pyroA4; methB3; riboB2 (chaA1*?)	This study
SWJ 238	*riboA1 yA2; nimO18*^{Dbf4}	SWJ
SWJ 280	*pyroA4; nimP22*$^{DNA\ Pol\ ε}$; *chaA1*	SWJ
SWJ 1841	*yA2; pyroA4; nimQ20*^{Mcm2}	SWJ
AMO 4573	*yA2; snxA1; nimO18*^{Dbf4}; *riboB2*	This study
AMO 4570	*pabaA1; wA2 snxA1; pyroA4; nimP22*$^{DNA\ Pol\ Epsilon}$; *chaA1*	This study
AMO 4574	*wA2 snxA1; pyroA4; nimQ20*^{Mcm2} (*yA2*?)	This study
tSWJ 4578	*yA2; ΔsnxA::pyroA nimX1*^{G225S}; *pyroA4; riboB2*	This study
	(*Kutr-L::pyrG*?)	
tSWJ 4460	*ΔsnxA::pyroA nimX2*^{F223L}; *pyroA4; methB3; riboB2*	This study
	(*pyrG89*? *Kutr-L::pyrG*?)	
tSWJ 4581	*pabaA1; wA2 ΔsnxA::pyroA nimX3*^{Y306H}; *pyroA4*	This study
	(*Kutr-L::pyrG*?)	

tSWJ 4854	*ΔsnxA::pyroA nimA5; pyroA4; riboB2*	This study
tSWJ 4855	*pabaA1; ΔsnxA::pyroA nimA5; pyroA4; riboB2*	This study
tSWJ 4856	*pabaA1; ΔsnxA::pyroA nimA5; pyroA4; riboB2*	This study
tJKK 4583	*pyrG89; snxA::GFP::pyrG; pyroA4 ΔnkuA::argB; nimO18*; *riboB2*	This study
tKLS 4653	*pyrG89; snxA::GFP::pyrG; pyroA4 (ΔnkuA::argB*?)	This study
tSWJ 4703	*pyrG89; wA2 nimX2*^{F223L} *snxA::GFP::pyrG; pyroA4* (*ΔnkuA::argB*?)	This study
SWJ 4737	*nimE6 snxA::GFP::pyrG; nicA2 (pyrG89*?)	This study
tKLS 4643	*pyrG89; wA2 snxA::mRFP::pyrG; pyroA4 (ΔnkuA::argB*?)	This study
SLS 12	*nimA5 snxA1 wA2; pyroA4*	This study
SLS 305	*yA2; nimT23 snxA::mRFP::pyrG; methB3; choA1*	This study
SLS 314	*yA2 alcA::GFP::tubA::pyr4; wA2 snxA::mRFP::pyrG; choA1 (pyrG89*?)	This study
LO 1578	*pyrG89; GCP3::mCherry::riboB*^{Af}; *nimE::GFP::pyrG*^{Af}; *pyroA4 ⊿nku::argB; riboB2*	Berl Oakley
SLS601	*snxA1 nimE::GFP::pyrG*^{Af}; *pyroA4 (pyrG89*?)	SLA
SLS602	ΔsnxA::pyroA nimE::GFP::pyrG^{Af}; *argB2::alcA::snxA::argB+*; *nicB8 (pyrG89*? *pyroA4*? ΔnkuA::argB? *methB3*?)	SLA
SLS603	*nimX2 nimE::GFP::pyrG*^{Af}; *pyroA4; nicB8* (*pyrG89*? *ΔnkuA::argB*? *methB3*?)	SLA
SLS102	*snxA1 nimX2 nimE::GFP::pyrG*^{Af}*; pyroA4 (ΔnkuA::argB*? *methB3*? *pyrG89*?)	SLA
tSWJ 4095	*riboA1; snxA1; argB2::alcA::snxA::argB+; pyroA4; chaA1*	This study
tSWJ 4096	*riboA1; snxA1; argB2::alcA::snxA::argB+; pyroA4; chaA1*	This study
tSWJ 4097	*riboA1; snxA1::alcA::snxA+::argB+; argB2; pyroA4; chaA1*	This study
tSWJ 5153	*riboA1; snxA1::alcA::snxA::argB* 9-exon cDNA; *argB2; pyroA4*; *chaA1*	This study
tSWJ 5154	*riboA1; snxA1; argB2::alcA::snxA::argB* 9-exon cDNA; *pyroA4*; *chaA1*	This study

tSWJ 5129	*riboA1; snxA1::alcA::snxA::argB* 11-exon cDNA; *argB2; pyroA4*; *chaA1* (39 nt 5' UTR precedes cDNA start codon)	This study
tSWJ 5291	*riboA1; snxA1; argB2::alcA::snxA::argB* 11-exon cDNA; *pyroA4*; *chaA1* (162 nt 5' UTR precedes cDNA start codon)	This study
tSWJ 5297	*riboA1; snxA1; argB2::alcA::snxA::argB; pyroA4; chaA1* (32 nt 5' UTR precedes cDNA start codon)	This study
tSWJ 4124	*riboA1; nimX2 snxA1; argB2::alcA::snxA::argB+; pyroA4; chaA1*	This study
tSWJ 4125	*riboA1; wA2 nimX2 snxA1; argB2::alcA::snxA::argB+; pyroA4* (*chaA1*?)	This study
tSWJ 4324	*(riboA1*?) pabaA1*; ΔsnxA::pyroA; argB2::alcA::snxA::argB+*; *pyroA4 ΔnkuA::argB (riboB2*?)	This study
tSWJ 4325	*(riboA1*?) pabaA1*; ΔsnxA::pyroA; argB2::alcA::snxA::argB; pyroA4 ΔnkuA::argB (riboB2*?)	This study
tSWJ 4326	*(riboA1*?) pabaA1*; ΔsnxA::pyroA; argB2::alcA::snxA::argB; pyroA4 ΔnkuA::argB (riboB2*?)	This study
tSWJ 5187	(*riboA1*?); *ΔsnxA::pyroA; argB2::alcA::snxA::argB; pyroA4*; *nicA2; (riboB2*?) *chaA1*	This study
tSWJ 5188	(*riboA1*?); *ΔsnxA::pyroA; argB2::alcA::snxA::argB; pyroA4; (riboB2*?)	This study
tSWJ 5189	(*riboA1*?); *ΔsnxA::pyroA; argB2::alcA::snxA::argB; pyroA4; nicA2*; (*riboB2*?) *chaA1*	This study
tSWJ 5190	*pabaA1; ΔsnxA::pyroA; argB2::alcA::snxA::argB; pyroA4; chaA1*	This study
dSWJ 3693	*riboA1*/+ +/*yA2*; *nimX2*-F223L/*nimX2*-F223L; *wA2*/+ *snxA1*/+; +/*pyroA4*; +/*methB3*; *nicB8*/+ (MDS 250 x SWJ 1604)	This study
EAK 5496	*riboA1; snxA2; pyroA4*	This study
EAK 5497	*riboA1; snxA2; nicA2*	This study
SWJ 5562	*pabaA1 riboA1; wA2 snxA2*	This study
tSWJ 5573	*pabaA1; wA2 snxA1; argB2; pyroA4 ΔnkuA::argB; riboB2 chaA1*	This study
tSWJ 5574	*pabaA1; snxA1; argB2; pyroA4 ΔnkuA::argB; riboB2*	This study
tSWJ 5567	*pyrG89 pabaA1; snxA1; Kutr-S::pyrG; snoA31; riboB2*	This study

SWJ 5581	*yA2; snxA2; pyroA4; nicA2*	This study
tSWJ 5583	*pabaA1; snxA2; pyroA4 ΔnkuA::argB; nicA2 (snoA31*?)	This study
tSWJ 5584	*pabaA1 yA2; snxA2; pyroA4 ΔnkuA::argB; riboB2*	This study
tSWJ 5179	*pabaA1 yA2; nimA1; pyroA4*	This study
KJ1	*nimA1 snxA1 wA2; riboB2*	This study
tLC 5590	*pabaA1; snxA*+::$(GA)_3$GFDGA::*myc9::riboB*; *argB2; pyroA4 ΔnkuA::argB; riboB2*	This study
tLC 5591	*pabaA1; snxA*+::$(GA)_3$GFDGA::*myc9::riboB*; *argB2; pyroA4 ΔnkuA::argB; riboB2*	This study
tLC 5594	*pabaA1; wA2 snxA1*:: $(GA)_3$GFDGA::*myc9::riboB*; *argB2; pyroA4 ΔnkuA::argB; riboB2 chaA1*	This study
tLC 5595	*pabaA1; wA2 snxA1*::$(GA)_3$GFDGA::*myc9::riboB*; *argB2; pyroA4 ΔnkuA::argB; riboB2 chaA1*	This study
tLC 5600	*pabaA1; snxA2*::$(GA)_3$GFDGA::*myc9::riboB*; *ΔnkuA::argB; nicA2; riboB2*	This study
tLC 5601	*pabaA1; snxA2*::$(GA)_3$GFDGA::*myc9::riboB*; *ΔnkuA::argB; nicA2; riboB2*	This study
dSWJ 3799	*+/pabaA1 riboA1/+ yA2/+; +/wA2; +/argB2* (SWJ 598 x PCS 439)	This study
dSWJ 5972	*+/pabaA1 yA2/+; +/wA2 ΔsnxA::pyroA/+; +/argB2; pyroA4/+; nicA2/+* (tSWJ 4394 x SWJ 598)	This study
dSWJ 3653	*riboA1/+ +/pabaA1; snxA1/+ +/wA2; +/argB2; pyroA4/+; choA1/+; chaA1/+* (SWJ 3406 x SWJ 598)	This study
dSWJ 5975	*+/pabaA1 +/biA1 yA2/+; snxA2/+; pyroA4/+; nicA2/+; +/riboB2 +/chaA1* (tSWJ 5581 x SWJ 4357)	This study
dSWJ 3923	*pabaA1/+ +/riboA1; wA2/+ snxA1/snxA1; +/pyroA4; +/choA1; +/chaA1 (drkA1/+*?) (SWJ 2862 x SWJ 3406)	This study
ΔsnxA/snxA1 heterokaryon	*yA2/+; ΔsnxA::pyroA/snxA1; pyroA4/+; nicA2/+; +/methB3; +/riboB2 +/chaA1* (tSWJ 4394 x SWJ 4030)	This study
ΔsnxA/snxA2 heterokaryon	*+/riboA1 +/pabaA1 yA2/+; +/wA2 ΔsnxA::pyroA/snxA2; pyroA4/+; nicA2/+* (tSWJ 4394 x SWJ 5562)	This study

SWJ, SW James

FGSC, Fungal Genetics Stock Center

SLA, Sarah Lea Anglin

SAO, Stephen A. Osmani

Table S2 PCR primers used in this study

A. *snxA* gene deletion[1,2]:

snxA 5-For	5’ TCT TTC TCT ACA TAT ATA CTC TGC AAG CAC TCA 3’
snxA 5-Rev	5’ CTC TCT CGC CAT TGT ATT TGT GGT ATA CTC GTA GTC GCC GTA AGG CAT TA 3’
snxA 3F	5’ GGT TCA TTC TTG TTA GGG TGT TCT GTG CAA TGT CTA CAA TAT GCT ACT CTG GCT TTG G 3’
snxA 3R	5’ TCG TTG ATA AGA TAA ATG TGG GAA GGT 3’
snxA Ne5F	5’ CGT ACT CGC TTT ACA ATA GCA GCA TT 3’
snxA Ne3R	5’ GGC TAT CCC AGA CCA GAG CAA CG 3

[1] *A. fumigatus pyroA* marker tails underlined
[2] snxA 5-For and snxA 3R were used in trans-locus PCR for molecular diagnosis

B. *snxA* C-terminal GPF/mRFP tagging[3,4]:

snxA-GSP1	5’ TGG CTT CGG AGG CTA TGG C 3’
snxA-GSP2	5’ CAT GAT CTG ATC CTG GGT AAG TCC 3’
snxA-GFP1	5’ GGA CTT ACC CAG GAT CAG ATC ATG GGA GCT GGT GCA GGC GCT GGA GCC 3’
snxA-GFP2	5’ GCT AAG CAG GGA AAC ACG CTA GTA CTG TCT GAG AGG AGG CAC TGA TGC 3’
snxA-GSP4	5’ TCT TGA AAC TGA CCG CCT CTC AT 3’
snxA NE-1	5’ GTC TCA AAC GTA AGT CTT TCC ATC C 3’
snxA NE-2	5’ CGC TCC TCG CAC GAA TCG 3’

[3] GFP/mRFP linkers underlined
[4] snxA GSP1 and snxA GSP4 were used in trans-locus PCR for molecular diagnosis

C. *alcA::snxA* overexpression construct:

alcA::snxA 5-FOR[5] 5' CTCA ACT AGT *GTC TTA* ***ATG*** *CCT TAC GGC GAC TAC GAG* 3'

alcA::snxA 3-REV[6] 5' CCTC GGA TCC *AAT GAG CAT AGT GAG ATG GAT AAA TAA CAA*

CAA C 3'

---

[5] *Spe*I site underlined; start codon in **bold;** *snxA* genomic DNA sequence italicized.
[6] *BamH*I site underlined; *snxA* genomic DNA sequence italicized.

D. Construction of $(GA)_3$GFGGA-myc9 epitope tag

myc-tandem FOR 5' GGT GCT GAA CAG AAA CTT ATT TCT GAA GAA GAT CTT

GGT GCT GAA CAG 3'

myc-tandem REV 5' AGC ACC AAG ATC TTC TTC AGA AAT AAG TTT CTG TTC

AGC ACC AAG ATC 3'

BspD1-linker-myc9 FOR[7] 5' CCTT ATC GAT *GGA GCT GGA GCA GGT GCG GGA TTC GAT GG***A** *GCT* GAA CAG AAA CTT ATT TC

myc9-Stop-HindIII REV[8] 5' TTCC AAG CTT ***TCA*** CTT GAT AGC ACC AAG **G**TC TTC TTC AGA 3'

---

[7] *BspD*I site underlined; $(GA)_3$GFDGA linker in italics; underlined and bolded **A** indicates a nucleotide change in order to improve specificity of amplification.

[8] *Hind*III site underlined; STOP codon in ***bold italics***; underlined and bolded **G** indicates a nucleotide change in order to improve specificity of amplification.

E. qRT-PCR:

actF: 5' TTC GGG TAT GTG CAA GGC 3'

actR: 5' TCG TGA CAA CAC CGT GCT 3'

snxA-q1[9]: 5' *AGA GAC TTC AAT CG*C CAA GTT CAC G 3'

snxA-q2: 5' GCT CTC GTG GCA CTG GTG TG 3'

snxA-q3: 5' CGG TAG GTT GGG CAT CAT CC 3'

---

[9] italics, exon 10; underlined, exon 11.